AD-A112 823 PENNSYLVANIA STATE UNIV UNIVERSITY PARK DEPT OF METE--ETC F/G 4/2
ESTIMATION OF VERTICAL WIND SHEAR FROM INFRARED AND MICROWAVE R--ETC(U)
JAN 82 H A PANOFSKY, A CAVALIER, J J CAHIR N00014-80-C-0115

UNCLASSIFIED NEPRF-CR-82-01 NL

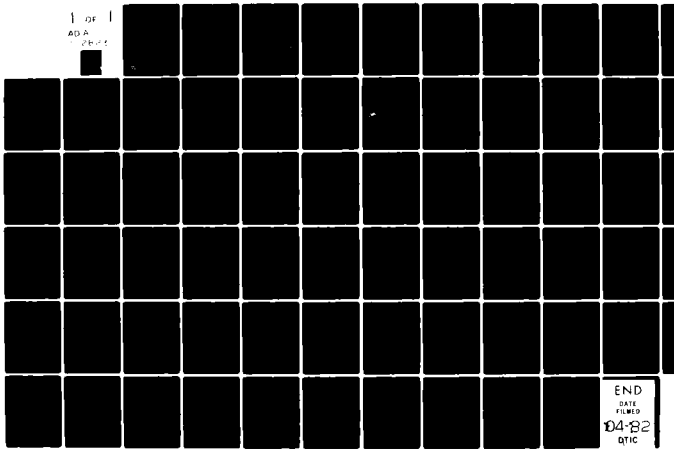

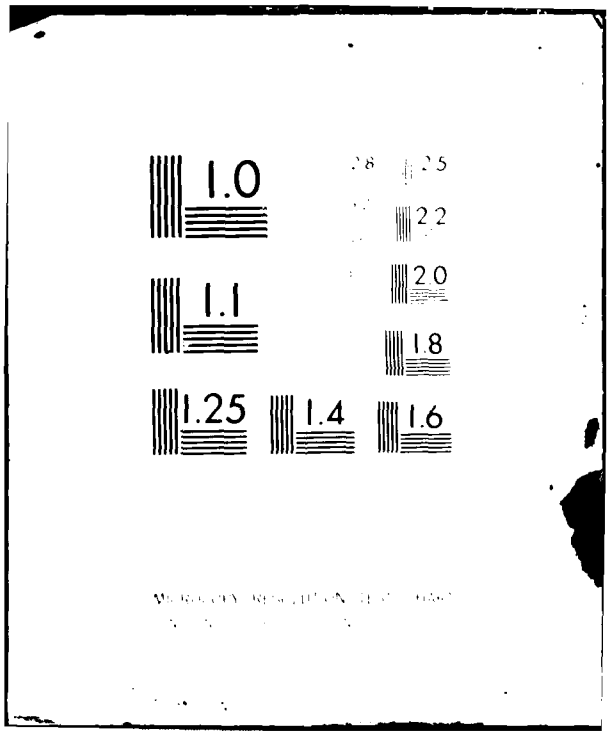
1.0
1.1
1.25
1.4
1.6
1.8
2.0
2.2

NAVENVPREDRSCHFAC
CONTRACTOR REPORT
CR 82-01

(12)

ESTIMATION OF VERTICAL WIND SHEAR FROM INFRARED AND MICROWAVE RADIANCES

Prepared By:

Hans A. Panofsky John J. Cahir
Anthony Cavalier Frederick Gadomski

The Pennsylvania State University
University Park, PA 16802

Contract No. N00014-80-C-0115

JANUARY 1982

APPROVED FOR PUBLIC RELEASE
DISTRIBUTION UNLIMITED

Prepared For:
NAVAL ENVIRONMENTAL PREDICTION RESEARCH FACILITY
MONTEREY, CALIFORNIA 93940

UNCLASSIFIED

SECURITY CLASSIFICATION OF THIS PAGE (When Data Entered)

(1.2)

REPORT DOCUMENTATION PAGE		READ INSTRUCTIONS BEFORE COMPLETING FORM
1. REPORT NUMBER NAVENVPREDRSCHFAC Contractor Report CR 82-01	2. GOVT ACCESSION NO.	3. RECIPIENT'S CATALOG NUMBER
4. TITLE (and Subtitle) Estimation of Vertical Wind Shear from Infrared and Microwave Radiances		5. TYPE OF REPORT & PERIOD COVERED Final 6. PERFORMING ORG. REPORT NUMBER
7. AUTHOR(s) Hans A. Panofsky, John J. Cahir, Anthony Cavalier & Frederick Gadomski		8. CONTRACT OR GRANT NUMBER(s) N00014-80-C-0115
9. PERFORMING ORGANIZATION NAME AND ADDRESS Department of Meteorology The Pennsylvania State University University Park, PA 16802		10. PROGRAM ELEMENT, PROJECT, TASK AREA & WORK UNIT NUMBERS PE 61153N PN RR033-02 TA 001 NEPRF WU 6.1-1
11. CONTROLLING OFFICE NAME AND ADDRESS Office of Naval Research Department of the Navy Arlington, VA 22217		12. REPORT DATE January 1982 13. NUMBER OF PAGES 76
14. MONITORING AGENCY NAME & ADDRESS(if different from Controlling Office) Naval Environmental Prediction Research Facility Monterey, CA 93940		15. SECURITY CLASS. (of this report) UNCLASSIFIED 15a. DECLASSIFICATION/DOWNGRADING SCHEDULE

16. DISTRIBUTION STATEMENT (of this Report)

Approved for public release; distribution unlimited.

17. DISTRIBUTION STATEMENT (of the abstract entered in Block 20, if different from Report)

18. SUPPLEMENTARY NOTES

Superseded AD-A100239
mc

19. KEY WORDS (Continue on reverse side if necessary and identify by block number)

Wind shear
Radiance gradients
Geostrophic wind
Satellite radiances

20. ABSTRACT (Continue on reverse side if necessary and identify by block number)

Linear regression estimates of radiosonde observed vertical wind shears between mandatory levels were made, using radiance gradients obtained via the TIROS-N satellite as predictors in a pilot experiment based on about 200-500 observations. The best results were obtained for shears between 850 mb and a level in the upper troposphere such as 300 mb. Results were similar for 850-400 or 850-200 mb shears, but notably inferior for 850-500 mb shears. The linear correlation coefficients between estimated (Cont. on reverse)

DD FORM 1 JAN 73 1473 EDITION OF 1 NOV 65 IS OBSOLETE
S/N 0102-014-6601

UNCLASSIFIED
SECURITY CLASSIFICATION OF THIS PAGE (When Data Entered)

Block 20, Abstract, Continued.

and smoothed observed components of shear was about 0.70, corresponding to about 50 percent explained variance in independent test samples. Somewhat higher explained variances (about 0.60) were achieved in a limited trial where the data-set was stratified according to subjectively-judged trajectory curvature.

Estimates of the wind itself in the upper troposphere were nearly as skillful as the best shear results. Overall, with the possible exception of curvature-stratified estimates in clear regions, both wind and wind shear estimates are not likely to be superior to methods that generate RMS wind errors of order 5 ms^{-1}.

Most of the information was contributed by the linear combination of microwave channel 2 minus microwave channel 3. Some additional information may be obtainable from the infrared (HIRS-2) channels 3, 4 and 5 (especially 5).

CONTENTS

LIST OF FIGURES

LIST OF FIGURES (continued)

LIST OF TABLES

Summary

This project was a pilot study aimed toward testing the hypothesis that vertical wind shear through the middle troposphere can be usefully estimated by linear combinations of satellite-sensed infrared and microwave radiance gradients. Linear regression estimates were made, with observed shears between mandatory levels as predictands and radiance gradients obtained via the TIROS-N satellite as predictors. Data observed during March 1979 over the western United States were used. Radiances were interpolated according to a neighboring-points slope-fitting analysis scheme to the radiosonde sites; the mesh-equivalence of the radiance data was about 250 km, so that synoptic scale radiance gradients were the predictors.

Data problems limited the sample sizes severely. Level 1B data, initially tested, were useless. Level 2A data for March 1979 contained no 1500 LST data, necessary for 0000 GMT comparisons over the western United States, at all. Further, the retrievals on individual days exhibit many missing data. Finally, cloudiness seriously limits the available data points for the infrared. As a result, the pilot experiments are based on about 200-500 observations apiece, which limits the confidence one can place in the conclusion. They must be considered very tentative.

The best results were obtained for shears between 850 mb and a level in the upper troposphere, such as 300 mb. Results were similar for 850-400 or 850-200 mb shears, but notably inferior for 850-500 mb shears.

The linear correlation coefficients between estimated and smoothed observed components of shear were about 0.70, corresponding to about 50 percent explained variance in independent test samples. Somewhat higher explained

variances (about 0.60) were achieved in a limited trial where the data-set was stratified according to subjectively-judged trajectory curvature.

In developmental trials, regression estimates of the wind itself in the upper troposphere were very similar in skill to the best shear results. However, these deteriorated somewhat in the independent trial on smoothed data, presumably because the shears contained more random error. Overall, with the possible exception of curvature-stratified estimates in clear regions, both wind and wind shear estimates are not likely to be superior to methods that generate RMS wind errors of order 5 ms^{-1}.

With respect to predictors, one result was quite consistent: Most of the information was contributed by the linear combination of microwave channel 2 minus microwave channel 3. Some additional information may be obtainable from the infrared (HIRS-2) channels 3, 4 and 5 (especially 5); indeed, the highest explained variances, and the best result in the curvature-stratified experiment involved *linear combinations of* the five microwave and infrared channels. Nevertheless, the HIRS channel results were disappointing. Even with a carefully checked set of clear points relatively free of interpolation errors, the infrared-only experiments did not match the microwave only experiments in skill. Part of the reason for this is stratospheric temperature gradient reversal, where the tropopause is low. This weakens the radiance gradients, especially in HIRS channels 3 and 4.

Further experiments are needed, on a much larger sample. Microwave channels 2 and 3, or microwave plus infrared channel 5 (or 3, 4 and 5) are the indicated predictors. Equations should be derived on unsmoothed wind shear observations but tested on smoothed ones. An objective method of stratification of trajectory curvature should be developed and tested. Finally, a rigorous test of standard errors of these estimates against those of alternative wind shear calculations should be made.

Estimation of Vertical Wind Shear from Infrared and Microwave Radiances

1. Introduction

The major purpose of the weather satellite program is to infer meteorological data from space, especially in regions of sparse observations. Estimation of winds presents special challenges, because satellites do not presently carry sensors specifically designed for wind measurement, although satellite-borne lasers are under consideration.

So far, winds have been obtained by use of three distinct methods: backscatter from the sea surface, tracking of cloud elements and computations from satellite-inferred temperatures.

Backscatter provides only surface winds, and is limited to oceanic areas. Cloud motions require the presence of clouds (which cover only about 50% of the earth's surface), and clouds may not travel with the speed of the wind. Further, cloud-tracing is only possible where distinct cloud elements, such as those produced by convection, can be identified in successive images. Lee (1979) showed that this technique is most useful in obtaining winds in the low troposphere, near 800 mb.

The technique of inferring winds from temperatures can be used in the largest volume of the atmosphere, and is most commonly applied. This approach can be considered to be operational, in the sense that the currently-applied operational forecasting models include wind analyses that are obtained from such calculations, at least over the oceans (Phillips et al., 1979). Although there have been some recent encouraging results reported by Phillips (1980), such wind estimates suffer from the weaknesses implicit in the recovery of the temperature profiles, which must

be estimated first in order to calculate the hypothetical balance between the wind field and the mass (temperature) field.

Recently Carle and Scoggins (1981) found that geostrophic winds calculated from satellite-derived mass fields display secondary wind maxima that are apparently spurious in the vicinity of the jet stream. Mean differences between satellite-derived and radiosonde-derived geostrophic wind speeds were of the order of 5 m s^{-1} and displayed standard deviations ranging up to 12 m s^{-1} near the jet stream in Carle and Scoggins' sample. They also found that the satellite-based geostrophic winds systematically underestimated the jet stream wind speed and its associated shear, consistent with the often reported tendency for satellite-based temperature soundings to underestimate the magnitude of the horizontal temperature gradient, where it is strong (Carle and Scoggins, 1981).

Recently, Brodrick (1980) produced an encouraging case-study of jet-stream winds on a cross section by calculating shear from temperatures observed by TIROS-N. Smith and Togstad (private communication) have studied a similar case to obtain a realistic jet stream mapping in a clear region. Also, Smith et al. (private communication) have detected small-scale temperature changes from a geostationary satellite, which might be useful in diagnosing small-scale wind shear.

Wind information derived from radiances has some drawbacks: 1) The vertical resolution is poor, 2) temperature information can be used directly only to infer balanced wind shears, not winds at any one level, 3) the transmission of infrared radiances is limited by clouds. Microwave radiances penetrate clouds (not precipitation), but the vertical resolution of microwave-derived winds is theoretically somewhat coarser than that obtainable from infrared-derived winds. Perhaps optimum results can be achieved by combination

of infrared and microwave radiances. 4) The derived wind shears are related to the mass field by theoretical relations which are subject to assumptions which may not be completely satisfied.

In practice, it is desirable to infer winds rather than wind shears from satellites. We can identify three distinct methods for obtaining winds, given the possibility of estimating wind shears.

In the first case, it is assumed that winds are available at a particular level from other information. For example, winds near 200 mb are quite well known from jet aircraft and cirrus motions. Or, winds near 850 mb may be available from motions of low-topped convective clouds. Combining these winds with satellite-derived wind shears yields winds at other levels.

Alternatively, it is assumed that the sea level pressure field is known from other information. Then, the satellite-derived temperatures yield the pressure field and hence balanced winds. This technique is being used successfully by NOAA at the University of Wisconsin, under the direction of Dr. William Smith.

Finally, winds are obtained statistically from wind shears. It is known empirically that wind shears between 1000 mb and 500 mb are quite well correlated with the winds themselves at 500 mb, at least in middle latitudes. Statistical relationships can be derived for these quantities. However, coefficients may have to be stratified by region and season.

In this project, we attempt to use the first and third of the methods above to infer winds from satellite radiance gradients. The use of horizontal radiance gradients is advantageous in that the effects of systematic error in the radiances are reduced.

2. Theory

Vertical wind shears were first derived from horizontal radiance gradients by Zak and Panofsky (1968) who used the relatively crude measurements on TIROS 7 to infer wind shears between 100 mb and 10 mb. They began by putting (for a given narrow wavelength band)

$$R = \int_0^\infty W(z)I(T,z)dz \quad ,$$

where R is the radiance, W(z) a weight function which depends on height z but is constant in the horizontal, and I is the contribution at each height to the total radiance. T is temperature and I is a function of temperature at height z.

Differentiating with respect to x, an arbitrary horizontal coordinate,

$$\frac{\partial R}{\partial x} = \int_0^\infty W(z) \frac{dI}{dT} \frac{\partial T}{\partial x} dz \quad . \tag{1}$$

A similar equation holds in the horizontal y direction, at right angles to x. If we assume geostrophic winds

$$\frac{\partial T}{\partial x} = \frac{fT}{g} \frac{\partial v}{\partial z} \quad , \tag{2}$$

where v is the velocity component in the y-direction, f is the Coriolis parameter and g is gravity. Then

$$\frac{\partial R}{\partial x} = \frac{f\bar{T}}{g} \int_0^\infty W(z) \frac{dI}{dT} \frac{\partial v}{\partial z} dz \quad . \tag{3}$$

Similarly,

$$\frac{\partial R}{\partial y} = - \frac{f\bar{T}}{g} \int_o^\infty W(z) \frac{dI}{dT} \frac{\partial u}{\partial z} dz \quad . \tag{4}$$

The functions $W(z)$ and $\frac{dI}{dT}$ are well known. Figure 1, taken from Smith et al. (1979), shows $W(z)$ for TIROS-N infrared and microwave channels used in this report. The problem is to solve (3) and (4) for wind differences between certain levels, given measured values of $\frac{\partial R}{\partial x}$ and $\frac{\partial R}{\partial y}$ in several channels simultaneously.

This problem has been discussed by many investigators. Of special interest here is the work by Fleming (1979) who showed that finite wind differences between particular levels can be obtained from linear combinations of radiance gradients in particular channels in the infrared region.

Such linear combinations can also be derived by regression analysis which assures the statistically "best" representation of observed wind differences or winds from a linear combination of radiance gradients. The drawback of the statistical method is that the fit may provide coefficients best suited only to the original (developmental) sample. Since they are not based on physical reasoning, they may not be equally well suited to other samples; hence it is essential that such equations be tested on independent information.

Equations (3) and (4) are based on the geostrophic assumption, and clearly lead to underestimates of wind shears in anticyclonic and overestimates in cyclonic regions. Because of this restriction, improved statistical relationships could be derived by developing separate equations in areas of contrasting curvature of the flow or by relating "errors" in the equations to contour curvature.

3. Satellite data

The radiance data for this study were obtained from the Satellite Data Services Division (SDSD) of the National Climatic Center (NMC). The TIROS-N satellite, launched in October 1978, was the source for all satellite data. To allow for several months of system shakedown time, the month of March 1979 was chosen for this pilot study.

The TIROS-N satellite is the first in a series of a new generation of NOAA operational polar orbiting satellites. The orbital period is approximately 102 minutes resulting in 14.2 orbits per day. The satellite operates with a southbound equator crossing time (descending node) at approximately 0300 Local Standard Time (LST) and a northbound equator crossing (ascending node) at approximately 1500 LST.

The satellite is equipped with an instrument package known as the TIROS-N Operational Vertical Sounder (TOVS) which consists of three instruments: 1) the second version of the High Resolution Infrared Radiation Sounder (HIRS-2), 2) the Microwave Sounding Unit (MSU) and 3) the Stratospheric Sounding Unit. Each instrument is a multi-channel radiometer which measures the radiation emerging from the top of the atmosphere. For this study of mid-tropospheric wind shear, only radiance data from HIRS-2 and MSU are used. Table 1, adapted from Smith et al. (1979), gives a synopsis of the characteristics of each of the various spectral channels used in this research. Only channels 2 and 3 of the MSU and 3, 4 and 5 of the HIRS-2 were used here, because only these channels respond significantly to temperatures in the middle troposphere (see Fig. 1).

The scan pattern of the HIRS-2 and MSU instruments for two consecutive orbits is shown in Fig. 2a. The HIRS-2 samples 56 fields of view (FOV) in a

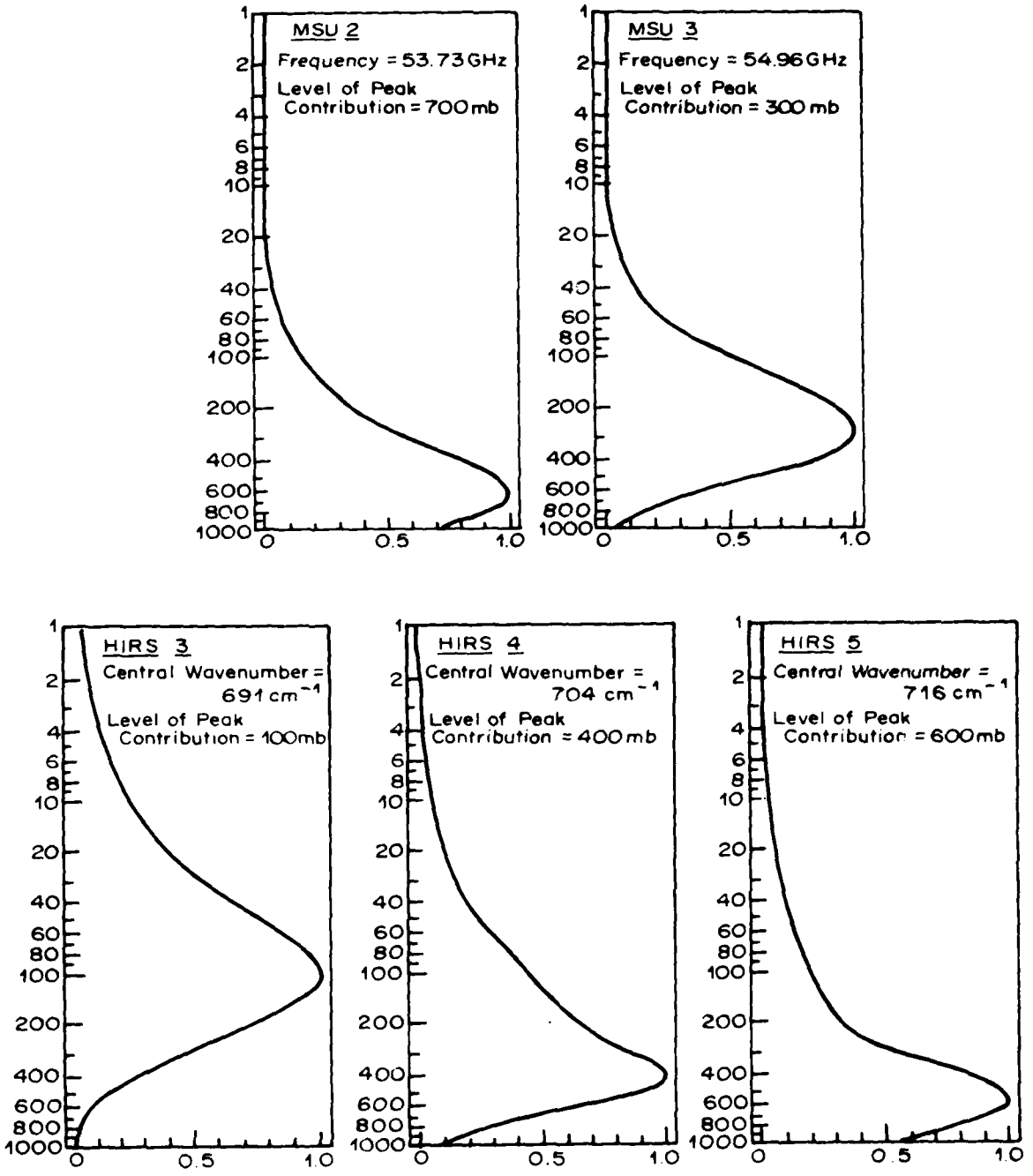

Figure 1. TOVS weighting functions for the channels used in this study.

HIRS Channel Number	Channel Central Wavenumber (cm^{-1})	Principal Absorbing Constituents	Level of Peak Energy Contribution
3	691	CO_2	100 mb
4	704	CO_2	400 mb
5	716	CO_2	600 mb

MSU Channel Number	Frequency (GHz)	Principal Absorbing Constituents	Level of Peak Energy Contribution
2	53.73	O_2	700 mb
3	54.96	O_2	300 mb

TABLE 1. Characteristics of TOVS sounding channels.

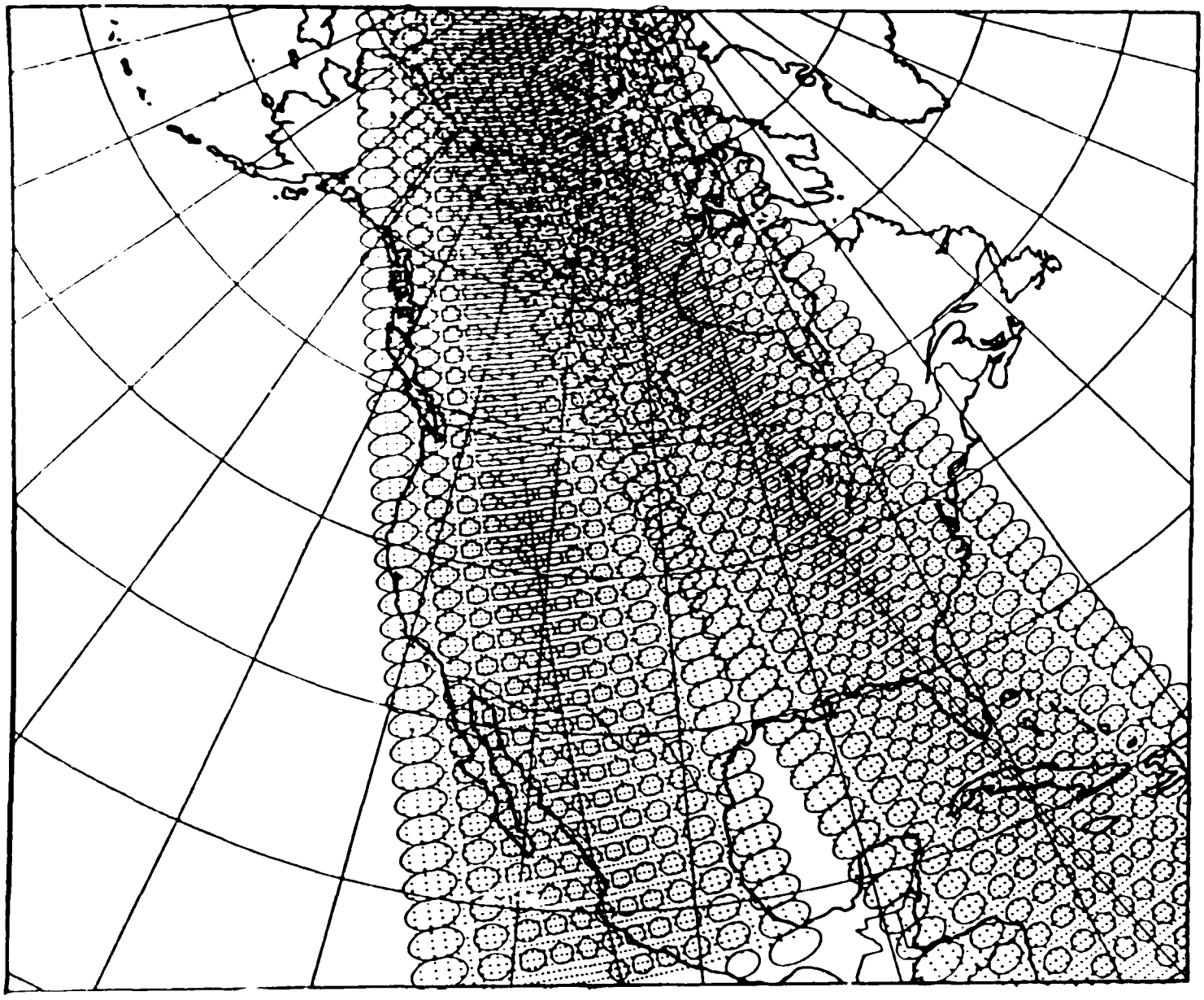

Figure 2a. HIRS and MSU scan patterns for consecutive orbits.

cross-track scan of 2240 km. The MSU samples only 11 fields of view having the same cross track linear extent, resulting in significantly lower horizontal resolution. The effective horizontal scales are shown on Fig. 2b.

In the data set obtained from SDSD for this study, the raw MSU measurements were corrected for slant path and surface emissivity effects. HIRS measurements were also corrected for limb and water vapor absorption effects. These data sources had been combined by interpolation of the lower resolution MSU measurements to the HIRS scan positions but the HIRS data retained greater resolution. Within the TIROS Atmospheric Radiance Module (TARM), these single field-of-view data were organized into "boxes" whose dimensions are nine scan spots across the satellite track by seven scan spots along the track. TARM then produced a single set of radiances in all spectral intervals of HIRS and MSU, which were estimates of the radiances in this 63 FOV area. Dimensions are shown on Fig. 2b. Thus, the horizontal resolution of the radiance data used in this study is approximately 250 km. If it is assumed that a $2\Delta x$ wave is at the detection level and a $10\Delta x$ wave is well resolved, then the infrared sounding could have detected horizontal scales of the order of 100-200 km in the initial data, but the processing has reduced that capability to about a 500 km scale. Similarly, the microwave soundings would, at best, detect horizontal structures with minimum scales of the order of 500 km, and data from both spectral intervals could only resolve well structures having characteristic horizontal length scales of approaching 2500 km. Thus, it could be expected that this analysis would produce errors associated with mesoscale structures, including strong fronts and their associated jet streams.

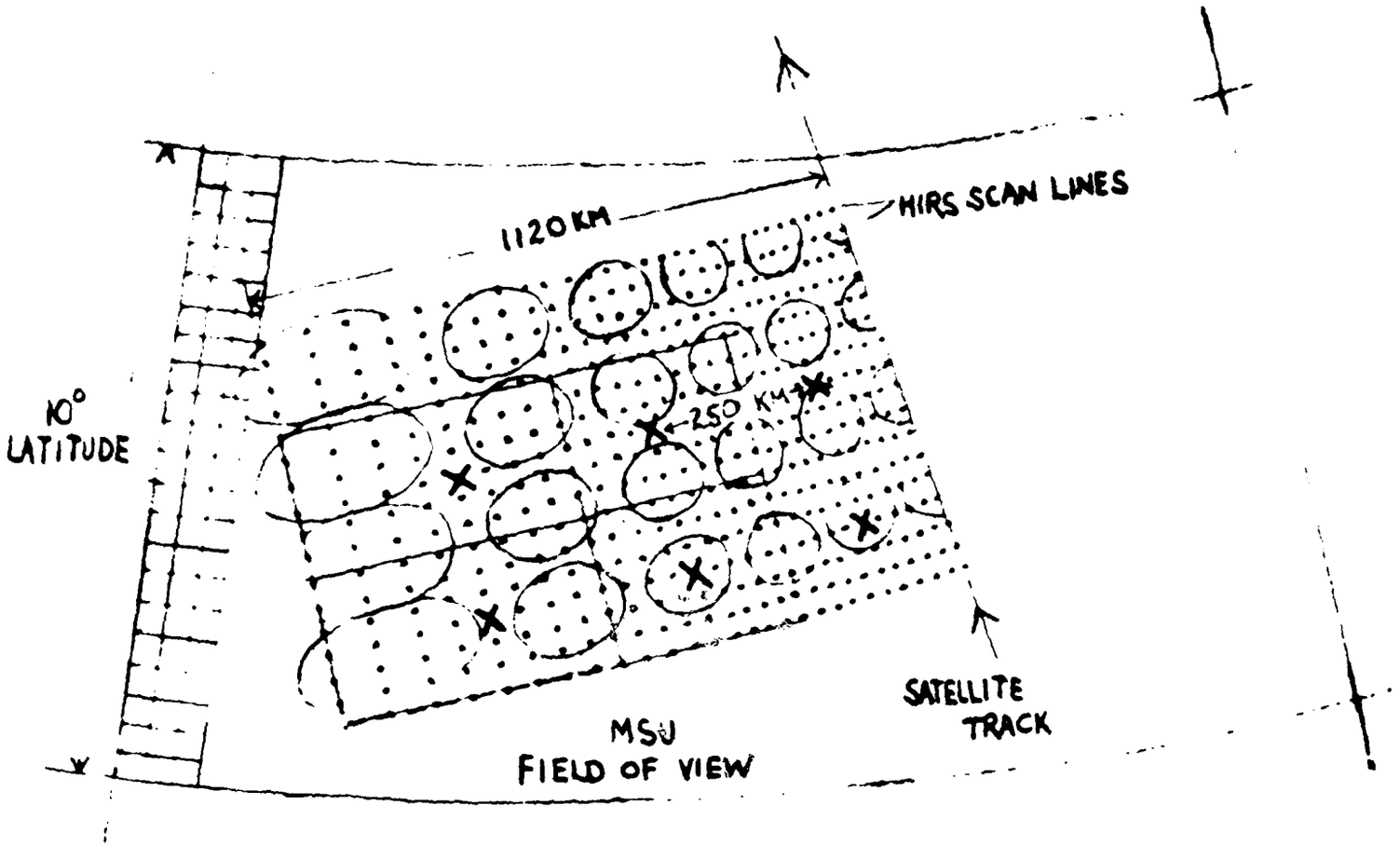

Figure 2b. Diagram of a portion of the TIROS-N satellite swath showing relative horizontal dimensions. Ellipses are MSU fields of view. Dots are HIRS fields of view. X's are the center of the seven scan line by nine scan spot boxes which TARM produces. The X's show the effective horizontal resolution of the radiance data used in this study. Also shown is a portion of the 50 km grid (produced by Surface II) onto which radiance data is interpolated so that gradients may be calculated.

Because many cloud structures have smaller dimensions than the scales discussed above, the smoothing of these data alleviates small-scale contamination by clouds at the expense of resolution. However, elimination of cloud-contaminated radiances also produces uneven spacing of the infrared radiance observations only. Infrared signals are subject to cloud contamination which makes the satellite infrared fluxes appear colder than they actually are. Within TARM, two methods are employed to correct for cloud contamination. In one, called the clear search method, sufficient holes are found in the clouds from whose uncontaminated measurements a volume estimate can be obtained. If this method fails, the N* approach is used, where physical and mathematical techniques are combined to obtain clear column radiances from the contaminated ensemble. Additional details concerning these methods are given by Smith et al. (1979); it is also discussed in Appendix A.

In cloudy areas, infrared radiances are quite unreliable. In the first sample, observations in these areas were deduced by interpolation. Later, a second sample of HIRS-2 data was tested in which seriously cloud-contaminated data were eliminated.

The TOVS sounding product tapes (Level 2A) used in this research contain brightness temperature data. These brightness temperatures are weighted, consisting of contributions through the depth of the atmosphere and are characteristic of the measured radiation at the top of the atmosphere. In order to test our hypothesis that horizontal radiance gradients relate information about vertical wind shears, these brightness temperatures were converted to radiances.

Information is extracted from the TOVS tapes in the form: DAY, TIME, LATITUDE, LONGITUDE and TEMPERATURE. Because of the asymmetry in the FOVs used for each box in the clear column radiance search, each latitude-longitude coordinate point represents a weighted central position in the seven scan line by nine scan spot box. In order to make the conversion to radiance, a slightly different algorithm for the channels of both sensors is used.

The microwave algorithms convert brightness temperature to radiance through the Planck radiation equation:

$$E = \frac{c_1 (\nu)^3}{\exp (\frac{c_2 \nu}{T}) - 1} \qquad (5)$$

where $c_1 = 1.190659 \times 10^5$ milliwatts per m^2 per steradian per cm^{-4}, $c_2 = 1.438833$ cm-°K, T is brightness temperature in °K, ν is the central wave number in cm^{-1} and E is the radiance in milliwatts per m^2 per steradian per cm^{-1}.

The generation of HIRS-2 radiance algorithms from brightness temperatures is similar. Here, however, band correction coefficients are applied to the apparent temperatures (T*) read from the tape, yielding the corrected brightness temperature T. The relation between T and T* is as follows:

$$T = \frac{T^* - b}{c} \qquad (6)$$

where T* and T are in °K, and b, c are band correction coefficients provided in

Table 2. The individual HIRS algorithms are then computed as before using (5). Table 2 lists the TIROS sensor algorithms used in this calculation.

Data sets on a latitude/longitude grid were created for each day and channel in the form: TIME, LATITUDE, LONGITUDE and RADIANCE. In order to test our hypothesis, a cartesian grid of horizontal radiance gradients was constructed with the Y axis along the satellite track. This necessitated a conversion of latitude-longitude coordinate radiances to a cartesian system.

This conversion is accomplished by the specification of two parameters. First the distance of the projected point from the pole is determined using the latitude angle and trigonometry. Second, the angular difference between the prime longitude and the longitude is computed, where the prime longitude is defined as the meridian which is perpendicular to the base of the map and which extends from the pole to the bottom of the map. These two parameters lay the framework for the conversion of latitude-longitude coordinate pairs to a cartesian grid on a polar-stereographic map with the Y axis oriented along the satellite track.

By specifying the desired number of grid points between the pole and the equator (100 was used here), a cartesian grid encompassing the North American radiosonde network west of 85° west was established with each grid point spaced about 100 km apart.

For use in this research, the geographic coordinates are the cartesian coordinates x, y defined by the satellite track, with radiance at each location constituting the independent variable (z). The only inherent restrictions are that the coordinate variables must be orthogonal and the z variable must be single valued.

Sensor	Channel Number	$\lambda^{-1}(cm^{-1})$	b	c	Radiance Algorithm
MSU	2	1.79	-	-	$E = \frac{6.85 \times 10^5}{\exp\{\frac{2.58}{T}\} - 1}$
MSU	3	1.83	-	-	$E = \frac{7.32 \times 10^5}{\exp\{\frac{2.64}{T}\} - 1}$
HIRS	3	691	.131	.99962	$E = \frac{3.83 \times 10^3}{\exp\{\frac{994.03}{T^*-.131}\} - 1}$
HIRS	4	704	.015	.99991	$E = \frac{4.148 \times 10^3}{\exp\{\frac{1012.21}{T^*-.015}\} - 1}$
HIRS	5	716	.010	.99993	$E = \frac{4.37 \times 10^3}{\exp\{\frac{1030.2}{T^*-.010}\} - 1}$

TABLE 2. Radiance algorithms and channel characteristics for TIROS sensors.

The basis for all operations in the analysis code of Surface II (Sampson, 1978) is a rectangular grid of values which is a numerical representation of the surface to be displayed. The grid is a numerical matrix whose elements are measurements of the z variable made at points identified by the geographic coordinates x and y. The geographic coordinates are defined by the rows and columns in the matrix.

Surface II has several provisions for estimating grids from irregularly spaced data. In fact, the gridding of scattered data points is the most important use of this analysis package. There are two general classes for estimating a regular mesh of points on a surface defined at other points, namely global and local fit techniques. Global estimates are based on all original data points on the surface while local estimates are performed only from a selection of nearby data points.

Local fit techniques are considered to be the best for estimating points on an irregularly shaped surface, since the estimate techniques are based on the premise that a nearby observation is a better estimate of the value at a point on a surface than a more distant one, and that a small number of the nearest control points provides essentially all of the information that is relevant to the estimate. Stated briefly, values at successive locations on a continuous surface are considered to be autocorrelated, with the degree of autocorrelation decreasing with increasing distance between the locations. This is essentially the same property employed by the Cressman method (Cressman, 1959) which is commonly used in meteorological work.

The versatility of Surface II is best illustrated by the varied ensemble of estimating procedures in grid construction available to the user. The standard method, and the one used in this study, is a two-part, weighted

average of the projected slopes from the nearest neighboring data points about each grid point. During the first pass, the slope of the surface is estimated at each data point. The search procedure finds the n nearest neighbors to the data point being considered and fits a weighted trend surface to the point. Weights inversely proportional to the distance from the data point being evaluated are assigned to the other points. Next, a constant of the fitted regression equation is adjusted in order to guarantee that the plane passes through the data point. If the search procedure does not find at least 5 points or if the simultaneous equations of the fitted plane have no solution, then the coefficients of a global trend are used as the local trend.

The second part of the method estimates the value of the surface at the grid nodes. A search technique locates n' nearest neighbor data points about each grid node. The x, y coordinates of the grid node are then substituted into each of the local trend-surface equations associated with these points. The result is a projection of these local surfaces to the grid node location. A weighted average of these estimates is then calculated with each slope weighted by the inverse of the distance between the grid node and the data point associated with the slope.

The weights which are assigned to the control points or the slopes at the points during the estimation procedure are allocated according to their distance away from the grid intersection being estimated. Several different weighting functions can be chosen, for example $\omega = 1/D$, $1/D^2$, $1/D^4$, $1/D^m$. The weighting function used in this research project is

$$\omega = [1 - \frac{D}{1.1\ D_{max}}]^2 / [\frac{D}{1.1\ D_{max}}]^2 \qquad (7)$$

where ω is the weight attached to a sample data point a distance D from the grid intersection being estimated. D_{max} represents the distance from the grid intersection to the most distant sample point in the set being used in the estimation.

In short, Surface II was used to calculate a cartesian grid matrix of interpolated radiances with the x, y axes defined perpendicular to and along the satellite track respectively. Then, through a centered-difference technique, Surface II generated a grid matrix of horizontal radiance gradients.

Surface II uses as input a particular day's data set in the form of I, J, RADIANCE points where I and J represent the cartesian coordinates on the polar stereographic map. Typically, this data set consists of 200 points covering the geographic area from 85° to 140° west longitude and from 20° to 70° north latitude. For our purposes, Surface II interpolates to a square grid 120 grid points on a side with each point spaced 50.03 km apart. From these data, radiance gradients were obtained over 2 grid intervals, that is, 100 km centered on the radiosonde stations. By rounding the latitude-longitude coordinates of each radiosonde station to the nearest .5 degree, the finely interpolated grid matrix produced by Surface II is guaranteed to intersect each radiosonde station. Hence, centered difference horizontal gradients are calculated by differencing adjacent radiance values about each radiosonde station both along and across satellite track.

Surface II utilizes several data checks of which the Statistical Analysis check is the most important. The Statistical Analysis check detects instabilities in the data, i.e., finds regions where both the search procedure is inadequate and the global trend coefficients may be erroneous due to rounding.

If instabilities are encountered, Surface II informs the user, then proceeds to calculate the desired grid matrix. In this project, these instabilities were encountered on a very few occasions only, when cloud contamination depleted greatly the number of radiance values for a particular data set. These cases, which occurred only with the most contaminated HIRS data sets, were eliminated from the study.

4. Radiosonde Data as Predictands

The ultimate aim is to pair interpolated horizontal radiance gradients with corresponding radiosonde wind shears so that regression analysis can proceed. Wind data used for determining the observed shears were obtained from radiosonde observations archived on tape at the Penn State Meteorology Department. Shears were calculated for each station by vector subtraction of mandatory-level (850, 700, 500, 400, 300, 250, 200 mb) wind data. These observed shears, as calculated, contain errors which may make them unrepresentative of the synoptic-scale wind shear. First, radiosonde instrument errors are present in any data sample. Moreover, there are irregularities due to short averaging time and negligible spatial averaging of the wind observations. Thus, the set of observed shears are affected by sub-synoptic scale motions. This unwanted "noise" contributes to the unexplained variance in the final statistical results.

Some thought was given to the possibility of using analyzed (smoothed) wind data as predictands. However, regression (least square) fits automatically produce the "best" fits to irregular data with random errors.

However, the purpose of the procedure is to derive smoothed fields. Therefore, the verifications of the regression equations can best be done with analyzed wind fields.

A prime consideration in the analysis of data for this study was the need to have the observed radiosonde data correspond as closely as possible in time with the satellite radiance data. Given the satellite equator crossing times of 0300 LST and 1500 LST and the radiosonde observation times of 0000 GMT and 1200 GMT, it was decided that the western United States and Canada would be chosen as the target region for this study. In this part of the world, 0000 GMT corresponds to 1500-1700 LST and 1200 GMT corresponds to 0300-0500 LST. As a result of satellite malfunctions, nearly all of the radiance data near the 0000 GMT radiosonde observation time were missing from the March 1979 data archive. This reduced the size of the data sample by approximately half; however, sufficient 1200 GMT satellite data were available to permit a pilot study.

There is a relatively high density of radiosonde stations in the United States portion of the area, but rather few in Canada. In the final calculations, up to 46 radiosonde stations west of 85 W and east of 140 W between 25 N and 70 N were used (Fig. 3). In that area, the time difference between satellite and radiosonde observations ranged from nearly exact correspondence at the western edge to about three hours difference at the eastern edge. Allowing for the usual early release of the radiosonde by about one hour, the time correspondence may have been slightly better.

5. Statistical Technique

All of the correlations and regressions presented in this paper were calculated through the use of the Statistical Analysis System, a commercially

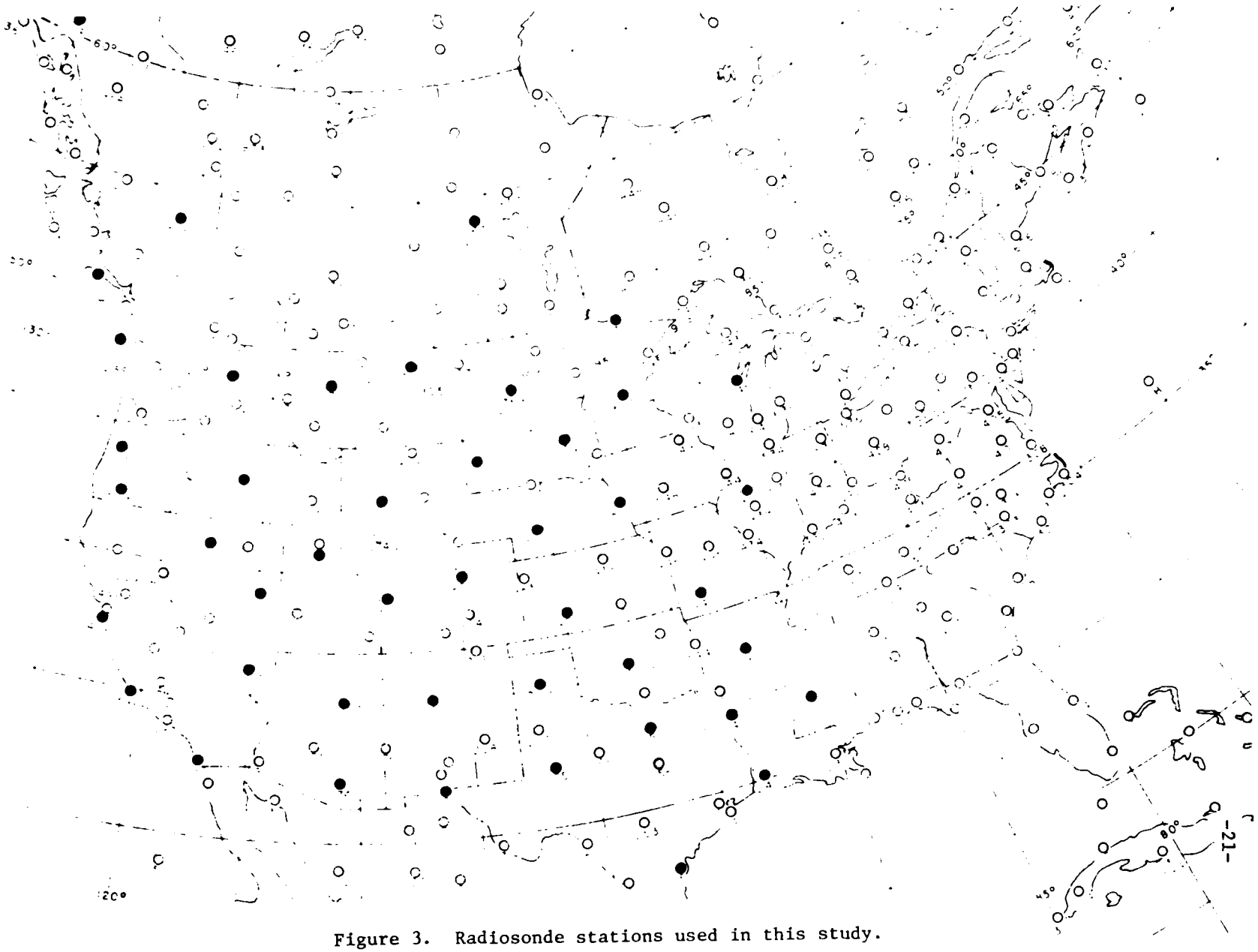

Figure 3. Radiosonde stations used in this study.

produced statistical package available at many IBM computer installations.

The procedure chosen to develop the linear regression equations was forward stepwise selection. In this method, the first predictor chosen is the one which has the highest correlation with the predictand. In each subsequent step of the selection process, the predictor chosen is the one which, when added to the equation, leads to the greatest reduction in variance.

Of major concern in the linear regression approach, is the determination of the optimum length of the equation. Including too many predictors in a regression equation can result in the overfitting of the equation to the developmental sample. As a rule, the smaller the developmental sample, the fewer should be the predictors allowed to enter the regression equation (Lorenz, 1977).

Statistical significance tests are often used to determine the cutoff point for the addition of predictors. However, such tests are not strictly applicable here because meteorological observations are not independent of one another. Weather typically occurs in regimes several thousand kilometers in length. Thus, the horizontal scale of systems far exceeds the distance between radiosonde observations. As a result, two separate radiosonde observations are not usually statistically independent.

The best available test for the reliability of an equation derived in these circumstances is an independent test of another set of data. In this pilot study, data from the first twenty-one days of March 1979 were used as the developmental sample. The last ten days of the month were set aside as the independent sample.

6. Experiments and Results

a. Characteristics of single channels

The early stages of data analysis for this study consisted of the preparation of many radiance maps for a single channel. Appendix B shows several examples of these radiance maps for each of the channels used in this study. This map preparation was done to gain insight into the relationship between the radiance and wind shear fields which would later be explored statistically. In this pilot study, it was decided that the microwave channels would be explored first since they are seldom contaminated and yield the larger data base for use in statistical analysis. MSU channel 2, whose weighting function peaks near 500 mb, was judged as being the most potentially useful single channel.

Figure 4 is a map of MSU channel 2 radiance contours together with arrows which show the calculated values of mid-tropospheric (700-400 mb) wind differences at 1200 GMT on 8 March 1979. The magnitude of the shear is proportional to the length of the wind arrow (see scale Fig. 4). The case is quite typical of many of the MSU channel 2 mappings. It can be seen that there is a generally good correspondence between satellite-derived contour orientation and observed 700-400 mb shears. In addition, information about the position of the mid-tropospheric jet appears to be present; tight radiance contour spacing from western Washington and Oregon into Wyoming is associated with large shear magnitudes in this region. The small shears in Montana and along the southern United States border are also linked with smaller radiance gradients in this region.

Figure 5 is a similar map based on data for 1200Z on 2 March 1979. This case is presented to highlight severe inconsistencies which appear occasionally between observed and satellite derived shears. Note that while

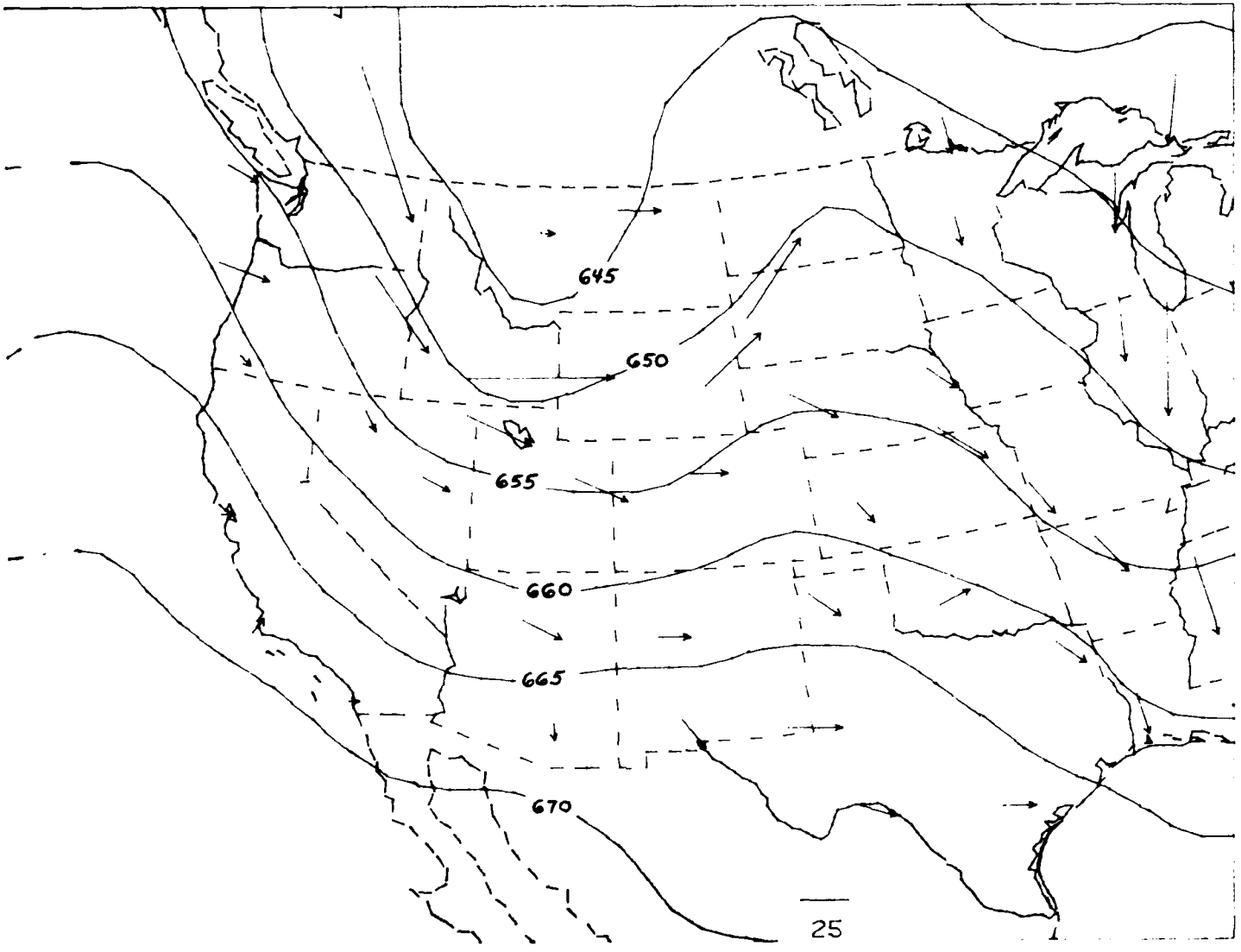

Figure 4. Radiance contours in milliwatts per m^2 per steradian per cm^{-1} ($x10^{-5}$), for descending node on 8 March 1979. 400-700 mb wind shear arrows (knots) for corresponding time (1200 GMT).

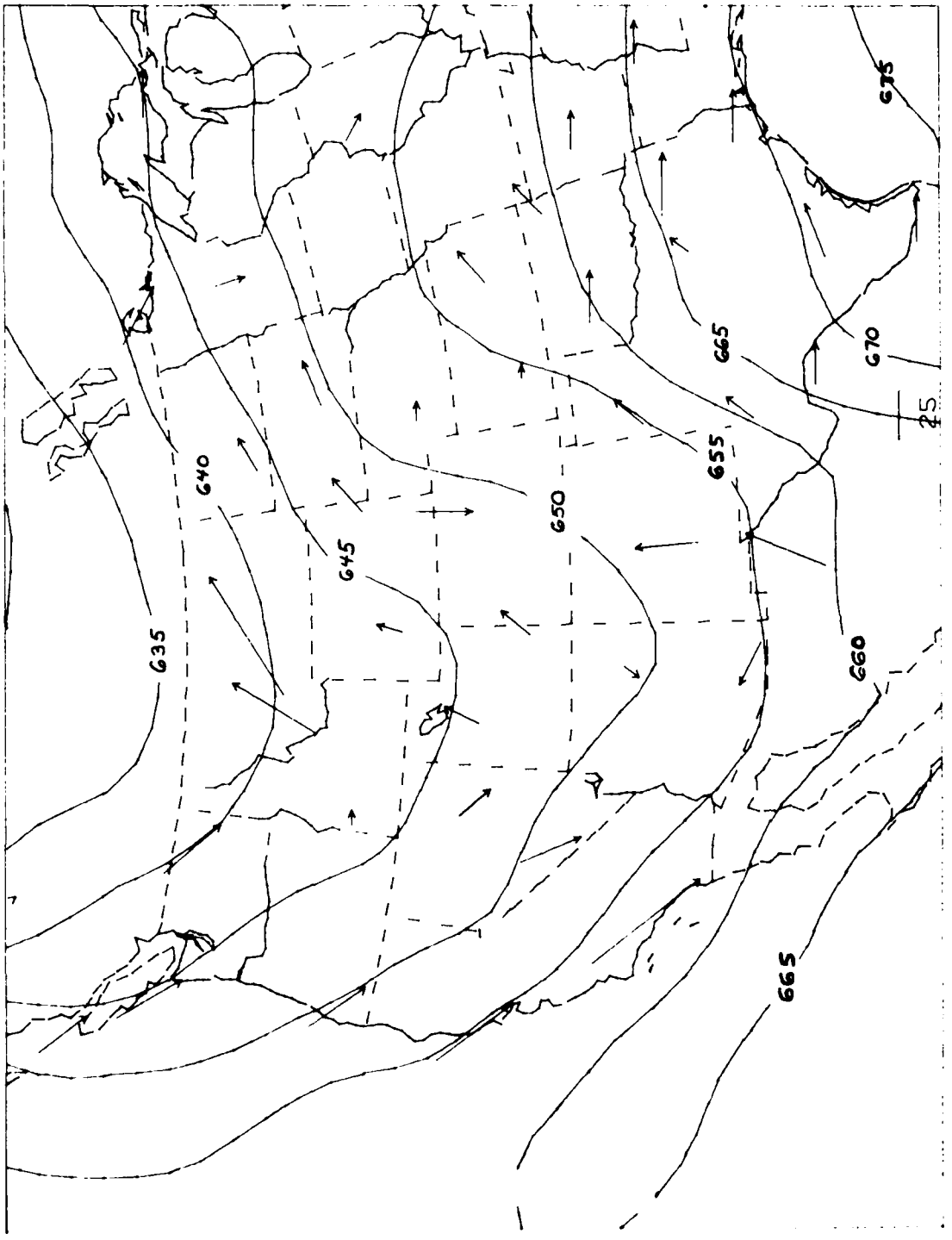

Figure 5. Radiance contours in milliwatts per m^2 per steradian per cm^{-1} ($x10^{-5}$), for descending node on 2 March 1979. 400-700 mb wind shear arrows (knots) for corresponding time (1200 GMT).

the overall patterns still correspond quite well, the observed shears at Winslow and Tucson, Arizona and at Denver, Colorado are nearly opposite of what would be expected from radiance contours.

The NMC analyses of the upper air conditions as well as the soundings from Tucson and Winslow were examined closely for this case. A portion of the analysis for 500 mb is shown in Fig. 6. A sharp trough axis through central Arizona is apparent. At lower levels a small pocket of cold air existed in southern Arizona and northern Mexico. It is probable that the scale of this sharp feature cannot be resolved with these coarse microwave data. Moreover, the strong cyclonic curvature of the streamlines at low levels appears to be decreasing with height, introducing a difference between the radiance gradient and the observed shear. The actual wind difference exceeds the thermal wind difference in flow becoming more anticyclonic upward and vice-versa; in any region of strong vertical change of curvature of the streamlines, systematic errors should appear.

If this is a case where sub-grid scale phenomena affect the observed shears, verification on smoothed rather than actual wind shear as the predictand should improve the agreement.

To give some quantitative idea of what can be obtained from a single microwave channel, a regression experiment was performed with MSU channels 2 and 3. The data set used was a subset of the 1-21 March 1979 developmental data sample consisting of 550 points on 19 days. In an effort to minimize the effect of the interpolation technique on the final results only those days with the greatest number of data points were used. Fractions of explained variance values were then calculated for many combinations of shear layers. Table 3 shows these values for the layers tested. Regression analysis (least squares) is used to fit smooth curves to "noisy" data. The "noise"

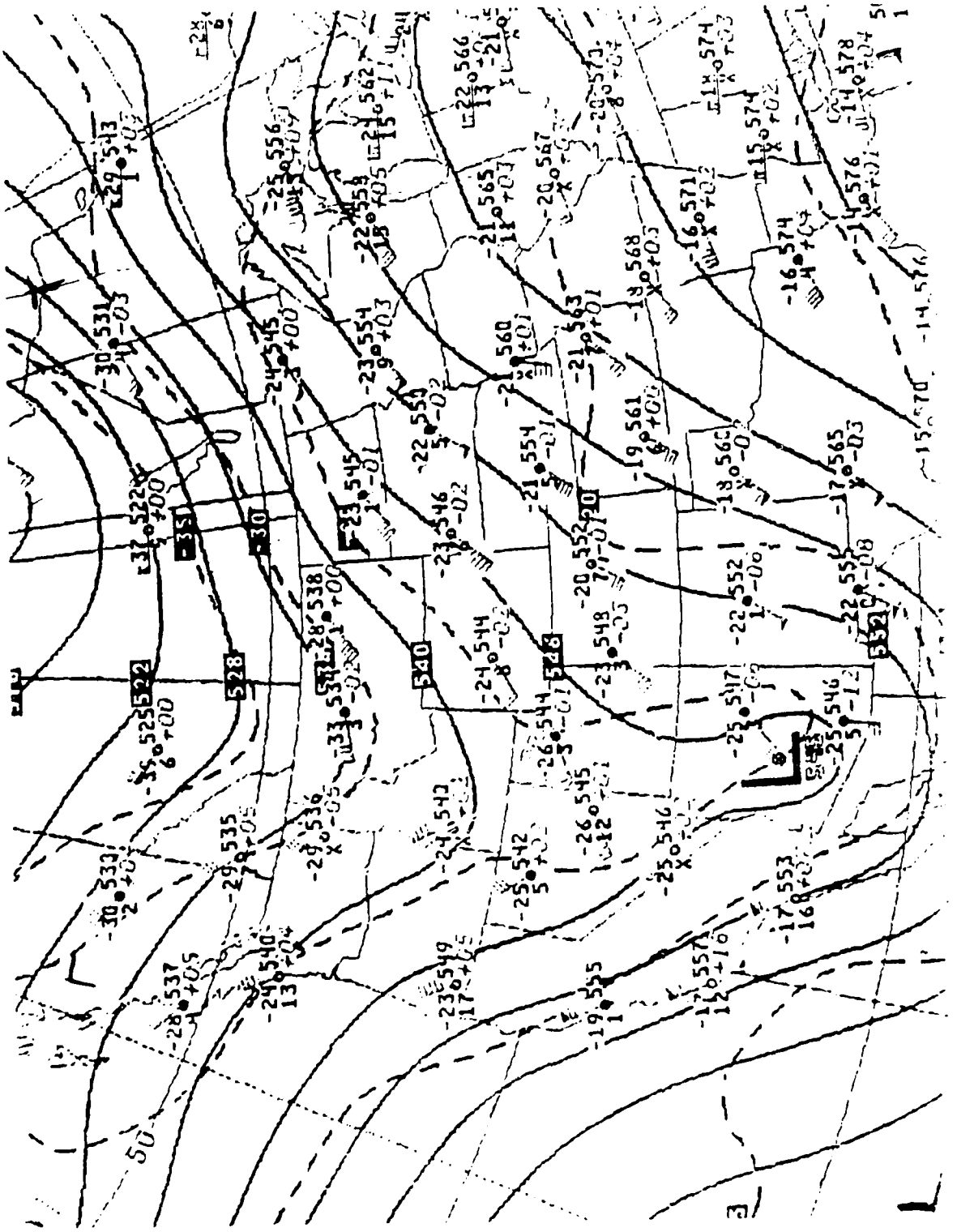

Figure 6. NMC 500 mb analysis for 1200 GMT, 2 March 1979.

then becomes part of the unexplained variance. There is no point to smooth the predictands first, because this smoothing is subjective, and reduces the degrees of freedom. For these reasons, we chose directly observed vertical differences of radiosonde wind components u and v as predictands, as well as u and v components at particular levels. Wind speed and direction are less satisfactory, because the significance of directions depends on speed; u and v have better statistical properties. Best results in channel 2 are obtained for shears between 850 mb and 300 mb, although 850-400 mb is nearly as good. It is seen, however, that 850-500 mb shears are not accounted for nearly as well by radiance gradients in this channel. The reason is clear: the weight function for MSU channel 2 peaks at 500 mb, so that the weights of the winds at the two levels peak above and below 500 mb, respectively. By contrast, channel 3 alone explains only a very small fraction of the variance of wind shear.

There is a tendency (possibly not significant) for the fraction of v components explained to be slightly larger than that of the u-components. But in this sample, the v-components have slightly larger total variances, so that their prediction error (see later section) tends to be larger.

Theoretically, HIRS channels should yield better results than MSU channels since the weighting functions associated with infrared channels have more sharply defined peaks. Hence, the HIRS channels were first tested independently of the MSU channels to explore this contention.

The loss of data in the sample, which was related to instrument failure and contamination of infrared signals by cloudiness, presented challenges in the analysis of the HIRS data. Unfortunately, certain aspects of the HIRS results presented here seem to be a result of these sampling problems.

Once again, a subset of the 21-day developmental sample was chosen such that only the most data rich days were included. Because of retrieval problems, in fact, observations from only 9 days were used with only 275

Layer	MSU 2 u	MSU 2 v	MSU 3 u	MSU 3 v
200 - 400	4	3	3	2
200 - 500	8	6	3	1
200 - 700	24	29	2	3
200 - 850	33	38	1	2
250 - 400	6	9	0	1
250 - 500	17	24	1	3
250 - 700	31	36	2	3
250 - 850	38	39	1	0
300 - 500	16	21	1	0
300 - 700	33	36	2	2
300 - 850	42	42	2	4
400 - 700	32	37	2	4
400 - 850	42	41	3	4
500 - 700	27	30	1	1
500 - 850	21	19	1	0
700 - 850	22	17	1	1

Table 3. Percent of Variance of Wind Shear Components Explained by MSU Channel 2 and MSU Channel 3 Radiance Gradients.

Number of Observations = ∿500

observations of each variable. See Table 4,which shows the days used in this analysis along with the number of grid values available on each day. Even on these days, only interpolated radiances were available over large areas, as a result of extensive cloudiness.

Table 5 shows a summary of the HIRS results. The explained variances are generally quite low, especially for channels 3 and 4. In fact, most of these quantities are probably not significantly different from zero! Examination of the data from these channels uncovers two points of interest. In spite of the choice of data-rich days, irregular distribution of data probably contributed to questionable interpolation at some locations. In addition, the magnitudes of the radiance gradients observed in these channels were generally much smaller than the MSU gradients. Weighting functions for these channels show significant contributions from both the upper troposphere and from the lower stratosphere. Stratospheric temperature gradients tend to be negatively correlated with tropospheric gradients underneath; hence, gradients in these channels are flattened which is reflected in the very weak gradients of these radiances. Correlations with channel 5 are not as bad as with 3 and 4, but as we shall see, not as good as with MSU channel 2. The difference could result from use of interpolated infrared radiances in cloudy areas, or from generally unreliable values in partly cloudy regions. In principle, MSU 2 and HIRS 5 should perform about equally well since their weight functions are very similar indeed (see Fig. 1).

b. Combination of 2 Microwave Channels

Next, regression equations were computed including just microwave channels 2 and 3 as predictors,since clouds do not influence the analysis. All but three days were used in this analysis (see Table 4).

MSU	# Grid Points	HIRS	# Grid Points
March 1	226 *	March 1	91
March 2	234 *	March 2	106 *
March 3	207 *	March 3	82
March 4	174	March 4	76
March 5	128	March 5	77
March 6	181 *	March 6	84
March 7	211 *	March 7	112 *
March 8	213 *	March 8	123 *
March 9	149	March 9	47
March 10	221 *	March 10	113 *
March 11	190 *	March 11	97
March 12	86	March 12	30
March 13	191 *	March 13	75
March 14	183 *	March 14	69
March 15	166 *	March 15	57
March 16	133 *	March 16	45
March 17	175 *	March 17	105 *
March 18	213 *	March 18	123 *
March 19	167 *	March 19	106 *
March 20	189 *	March 20	118 *
March 21	190 *	March 21	113 *

* Denotes Data used in Developmental Sample

Table 4. Characteristics of MSU and HIRS Datasets for Each Day in Developmental Sample Period.

LAYER	HIRS 3 u	v	HIRS 4 u	v	HIRS 5 u	v
200-400	0	0	6	0	2	1
200-500	2	1	7	0	7	0
200-700	10	8	6	0	13	10
200-850	12	9	8	0	24	11
250-400	3	2	9	1	13	3
250-500	7	5	9	1	20	5
250-700	14	11	7	1	22	17
250-850	16	11	10	0	34	16
300-500	5	6	4	0	18	6
300-700	12	12	4	0	19	17
300-850	18	13	6	0	30	16
400-700	14	12	1	0	12	18
400-850	22	12	2	0	22	21
500-700	11	11	1	0	7	20
500-850	18	11	2	0	17	20
700-850	11	4	0	0	11	6

Table 5. Percent of Variance of Wind Shear Components Explained by HIRS Channels 3, 4, 5 Radiance Gradients. Number of Observations = ∿280.

The results for these 2 channels as obtained from the developmental sample are shown in Table 6. Clearly, when compared to the results presented in Table 3, it is seen that channel 3 contributes significantly to the explained variances.

The equations derived for this test were:

$$USH3085 = 6.8 + 204\ MSU2 - 159\ MSU3$$

$$VSH3085 = -\ 0.9 + 184\ MSU2 - 162\ MSU3$$

$$USH4085 = 6.2 + 144\ MSU2 - 150\ MSU3$$

$$VSH4085 = -\ 2.8 + 146\ MSU2 - 128\ MSU3$$

$$U30 = 12.7 + 189\ MSU2 - 184\ MSU3$$

$$V30 = 2.6 + 203\ MSU2 - 217\ MSU3$$

$$U50 = 10.6 + 102\ MSU2 - 184\ MSU3$$

$$V50 = 1.3 + 129\ MSU2 - 170\ MSU3$$

where USH and VSH are shears between the mandatory levels indicated, in knots, and predictands of the form U and V are components of the observed winds at a single level, also in knots. The units of MSU2 and MSU3, which are the radiance gradients from the two microwave channels, are milliwatts per m^2 per steradian per cm^{-1} per 100 km.

Of course, the coefficients in these equations can be regarded as weights by which the radiance gradients have to be multiplied. It is clear that these weights have the correct signs: the weights are positive for MSU2, because this channel describes the major temperature field which is related to the wind shears. But MSU2 gradients are also influenced by temperature gradients higher up; these influences are removed by subtraction of quantities involving MSU3 gradients.

LAYER	MSU 2 + MSU 3	
	u	v
200-400	11	8
200-500	16	6
200-700	28	34
200-850	36	42
250-400	8	10
250-500	20	27
250-700	36	41
250-850	42	41
300-500	18	23
300-700	38	41
300-850	46	49
400-700	36	45
400-850	47	49
500-700	29	32
500-850	23	20
700-850	24	19

Table 6. Percent of Explained Variance for a Combination of Microwave Channels 2, and 3. Observations = $\sim$ 550.

c. Combinations of Microwave and Infrared Channels

Experiments were next performed in which two MSU and three HIRS channels were combined in a stepwise regression procedure in which observed wind shears were the predictands. Because HIRS coverage was poor on some days, only 9 days were used.

Table 7 summarizes explained variances and standard errors of estimates (in parentheses) for these experiments. All possible shears between mandatory levels in the 850-200 mb domain were tested, but only the layers displaying the best correlations are included in Table 7 along with other layers of interest. The highest correlations result for wind shears involving 850 mb, with the other level being in the upper troposphere. Infrared channels alone are disappointing; adding MSU 2 to them is helpful. The further addition of the infrared channels, increases the explained variances, but the standard errors do not decrease significantly by inclusion of the infrared channels. The smallest standard errors result for the 700-400 mb shears and the 850-250 mb shears, because of their smaller variability in our sample. Standard errors are likely to vary more among samples than correlations.

The rather poor performance of the infrared channels, particularly HIRS 2, could be due to use of interpolated values in cloudy regions. To test this possibility, another sample was collected from all 21 developmental days, but restricting the analyses only to areas were the HIRS coverage was good. The statistics did not improve substantially. This result indicates that the poor performance of HIRS channels must be due to the unsatisfactory retrieval techniques even in only partly cloudy areas. Overall, the results are not likely to be superior to alternative methods that generate root-mean-square wind errors of order 5 ms^{-1}. Also, as with MSU2 alone, the results involving

LAYER	MSU 2; 3		HIRS 3, 4; 5		MSU 2 HIRS 3, 4, 5		MSU 3 HIRS 3, 4, 5		MSU 2, 3 HIRS 3, 4, 5	
	u	v	u	v	u	v	u	v	u	v
200-500	15(18)	6(17)	9	1	16	7	15	3	20(18)	8(16)
200-700	25(20)	27(17)	19	12	32	27	20	13	33(18)	28(16)
200-850	34(23)	36(22)	26	13	45	34	27	15	46(19)	36(17)
250-700	32(21)	41(20)	27	19	41	37	27	24	42(19)	42(19)
250-850	36(17)	44(16)	36	19	53	38	38	24	55(13)	44(16)
300-500	18(25)	24(22)	17	9	26	23	19	12	27(24)	26(21)
300-700	36(20)	43(22)	23	21	41	38	25	26	43(19)	43(22)
300-850	44(22)	47(24)	33	19	55	40	37	25	57(20)	47(24)
400-700	32(14)	43(16)	22	19	35	37	23	24	38(14)	44(16)
400-850	45(19)	46(20)	34	27	53	40	36	29	56(15)	47(20)
500-850	46(22)	37(20)	25	21	45	32	28	27	47(19)	39(17)

Table 7. Percent of Variance of Wind Shear Components Explained by HIRS and MSU Stepwise Regressions. Standard errors in parentheses (knots). Number of Observations ≈ ∿ 275.

the 500 mb level are notably inferior to those involving 400 mb and higher levels.

It is noteworthy that the explained variance of the east-west component is larger than that of the north-south component in the cases where infrared predictors are used. This reverses a slight v-component superiority for the MSU2 predictor test reported in Table 3. That was explained in terms of somewhat greater u-component variability in the sample. A direct comparison cannot be made here, however, because the sample size has changed. However, it is worth noting that the standard deviations of u-components in this smaller sample average 4 to 6 knots less than the standard deviations of the v-components. It is believed that these differences are an artifact of the sample, and not of the atmosphere.

In middle latitudes, there tends to be a strong correlation between the wind shear and the wind itself at the higher altitude levels. For example, the 500-1000 mb shear is usually dominated by the 500 mb wind. In the preceding analyses, the 850-300 mb shear has exhibited relatively high correlations with radiance gradients. This suggests the possibility of estimating winds directly at a level in the upper troposphere from radiance gradients.

Thus, experiments were performed correlating the observed winds with radiance gradients for several mandatory levels. Results are summarized in Table 8. The general pattern of previous results remains the same; MSU channels 2 and 3 contribute the bulk of the information. The 300 mb winds are correlated with the radiance gradients of these channels. Indeed, the results are almost as good as those obtained for the 850-300 mb layer. Theoretically, wind shears should be predicted more accurately than single level winds. However, shears are noisier than the winds themselves and this may cancel the

Level	MSU 2		MSU 3		MSU 2,3		HIRS 5		MSU 2 HIRS 3,4,5		MUS 3 HIRS 3,4,5		MSU 2,3 HIRS 3,4,5	
Level	u	v	u	v	u	v	u	v	u	v	u	v	u	v
200	39	39	0	8	40	45	17	14	45	42	23	31	44	47
250	37	42	3	12	41	51	24	17	45	44	31	35	48	52
300	34	41	8	13	43	51	21	17	48	43	30	37	48	53
500	28	38	11	17	41	52	12	18	33	43	26	42	43	53

Table 8. Explained Variance for Single Levels

Number of Observations = $\sim$ 275

theoretical advantage. Thus, these results suggest the possibility of obtaining winds at a level statistically from radiance gradients. Coefficients, however, may have to be stratified by region and season.

d. Independent Tests

Because of the small sample size, it is essential to test the equations on independent data. This was done from data taken during the last 11 days of March, for which nine provided satisfactory data in the HIRS channels.

The equations were tested by two methods: in the first, raw shears were computed by vector differences of mandatory-level winds just as they had been in the developmental sample. The Cartesian components were then correlated with values predicted by the above equations.

Since the equations led to smoothed fields, they were also tested on horizontally smoothed observations. This smoothing was accomplished by a Cressman analysis scheme on a 30 x 40 grid (grid spacing approximately 90 km) which was overlaid on a polar stereographic map of the target area. Also a pass was made with a 1-4-1 smoother. Table 9 shows the results.

There is a considerable loss of explained variance as one goes from the developmental sample to the unsmoothed independent sample. This, of course, is typical of independent testing of regression equations. Interestingly, however, results improve by a larger amount when the equations are tested on the smoothed sample. This is not surprising since regression should handle the noise in the developmental sample in an optimum fashion. However, this improvement is less for the winds than the wind shears, since winds have less random error. Caution must be used in generalizing from this independent test due to the small size of the developmental and independent samples.

Nevertheless, the last section in Table 9 is likely to give the best idea how well regression is likely to predict winds and wind shears from MSU

Developmental Number of Observations = ∿ 275

Layer/Level	MSU 2,3 u	MSU 2,3 v	MSU 2,3 + HIRS 3,4,5 u	MSU 2,3 + HIRS 3,4,5 v
300 - 850	44	47	57	47
400 - 850	45	46	56	47
300	43	51	48	52
500	41	52	43	53

Independent (unsmoothed) Number of Observations = ∿ 190

Layer/Level	MSU 2,3 u	MSU 2,3 v	MSU 2,3 + HIRS 3,4,5 u	MSU 2,3 + HIRS 3,4,5 v
300 - 850	37	40	44	43
400 - 850	38	39	44	42
300	37	43	42	45
500	36	41	39	44

Independent (smoothed) Number of Observations = ∿ 190

Layer/Level	MSU 2,3 u	MSU 2,3 v	MSU 2,3 + HIRS 3,4,5 u	MSU 2,3 + HIRS 3,4,5 v
300 - 850	48	52	52	54
400 - 850	46	48	53	51
300	43	46	43	46
500	45	46	40	44

Table 9. Independent Tests on Two-Channel and Five-Channel Models.

data only, in middle latitudes. Further improvement should be possible by correcting for the deviation of actual from geostrophic winds.

Without such correction, then, we expect to account for about 50% of the variances of middle-troposphere layers, and somewhat less for the winds themselves, by the statistical techniques (correlations of order 0.7).

e. Correction for Contour Curvature

The actual wind difference should be less than the thermal-wind differences in cyclonic flow and vice versa. We should be more successful in wind shear estimation if we stratify our sample according to streamline curvature.

To gauge the effect of such stratification, the pilot study data were further subdivided into groups with strongly cyclonic, strongly anticyclonic, and nearly straight flow. The stratification procedure was subjective, based on NMC upper-air analyses.

Table 10 presents the results. Some conclusions are: 1) The subset which includes just straight flow generally shows considerable increases in explained variance over the full data set. 2) In the cyclonic and anticyclonic cases, only estimation of the u-components shows improvement due to stratification. This would be expected from the gradient-wind equation. 3) Generally, there was considerable improvement for the straight flow stratification.

We therefore performed a test to see whether the differences in the equations were physically reasonable. In particular, the anticyclonic equation should yield stronger winds and wind shears for the same input than the equations for straight flow. However, this did not turn out to be the case, so that the anticyclonic equations are probably not reliable.

Layer or Level	Cyclonic				Anticyclonic				Straight				All			
	MSU 2,3		MSU 2,3 HIRS 3,4,5		MSU 2,3		MSU 2,3 HIRS 3,4,5		MSU 2,3		MSU 2,3 HIRS 3,4,5		MUS 2,3		MSU 2,3 HIRS 3,4,5	
	u	v	u	v	u	v	u	v	u	v	u	v	u	v	u	v
300 - 700	.35	.37	.39	.45	.46	.44	.50	.47	.44	.49	.52	.54	.36	.43	.43	.43
300 - 850	.48	.44	.56	.57	.45	.47	.63	.48	.58	.56	.65	.64	.44	.47	.57	.47
400 - 700	.31	.33	.38	.36	.36	.35	.36	.38	.44	.57	.50	.61	.32	.43	.38	.44
400 - 850	.49	.44	.55	.51	.53	.47	.65	.49	.56	.54	.72	.58	.45	.46	.56	.47
500 - 850	.50	.39	.54	.43	.39	.38	.48	.38	.49	.41	.63	.47	.39	.37	.47	.39
250	.45	.46	.54	.51	.41	.39	.51	.40	.41	.55	.47	.64	.41	.51	.48	.52
300	.50	.44	.53	.50	.46	.49	.54	.51	.43	.54	.51	.62	.43	.51	.48	.52
500	.48	.44	.50	.46	.34	.46	.40	.46	.38	.56	.50	.65	.41	.52	.43	.53
	Number of Observations = ∿ 100				Number of Observations = ∿ 65				Number of Observations = ∿ 100				Number of Observations = ∿ 275			

Table 10. Summary of Explained Variances - Stratification Tests

In contrast, comparison between the equations for cyclonic and straight flow suggested reasonable behavior of the respective equations. In this experiment, we estimated mean wind shear and wind components from means of MSU 2 and 3 radiance gradients. In all cases, the predicted values were less in the cyclonic than the straight-contour sample.

7. Summary and Conclusions

This report is a pilot study, based on data from March 1979. Regression equations were developed and tested which led to estimates of winds and vertical wind shears, given horizontal gradients of radiances in various infrared and microwave channels. Due to the small sample, the results must be considered highly tentative.

The project suggests these conclusions:

1) In spite of their slightly better vertical resolutions, infrared radiance gradients show very little skill for estimation of synoptic-scale wind shears centered in the middle troposphere. Microwave gradients are generally superior. The improvement due to the addition of infrared information may not be statistically significant. Therefore, and because microwaves are relatively insensitive to clouds, we recommend that large-scale wind properties be estimated on the basis of microwave radiance gradients only. Infrared data should be used only in areas of limited cloudiness.

2) Without stratification by curvature of the flow, radiance gradients can account for about 50% of the variances of the shears in the middle troposphere (e.g., 300 mb to 850 mb), provided the observations are smoothed. A very limited experiment suggests that these variances can be increased to 60% if curvature and infrared channels are included. Standard errors of estimate for some of the results should be reducible to 15 knots or less.

3) The regression equations performed almost as well on the winds themselves as on wind shears. However, if we base the verification on smoothed fields, shear estimations are improved more than wind estimation.

4) The weights derived statistically have physically reasonable signs.

5) It is not clear whether the results are satisfactory for practical use. Such a decision requires comparison of the accuracy of statistical techniques with that of physical techniques.

8. Suggestions for Future Work

The results discussed here are tentative, because of the small sample involved. A significantly larger sample is needed to test the practical utility of the regression techniques.

On this larger sample, the following tests are suggested.

1) Test infrared and microwave predictors always in the same common periods, in areas of few clouds only.

2) Test the equations primarily on smoothed observations (although they must be derived from unsmoothed observations).

3) Handle curvature by developing equations between curvature effect and errors of the equations derived without allowing for curvature.

4) Test all equations on an independent sample.

5) Compare the standard errors of statistical techniques with standard errors of physical techniques, on the same set of data.

REFERENCES

Brodrick, H. J., 1978: The relationship between vertical sounder radiances and mid latitude 300 mb flow patterns. J. Appl. Meteor. 17, 477-481

Brodrick, H. J., 1980: Structure of a baroclinic zone using Tiros-N retrievals. Preprint Vol., Eighth Conf. on Wea. Forecating and Anal. Denver, Co. 129-134.

Carle, W. E., and J. R. Scoggins 1981: Determination of wind from Nimbus 6 satellite sounding data. NASA Reference Publication 1072. Texas A & M Univ. College Station, TX. 72 pp.

Cressman, G. P., 1959: An operational objective analysis system. Mon. Wea. Rev. 87, 367-374.

Douglass, A. R. and J. L. Stanford, 1980: The relationship between the gradient of satellite-derived radiance and upper tropospheric/lower stratospheric winds. J. Appl. Meteor. 19, 113-115.

Fleming, H. E., 1979: "Determination of vertical wind shear from linear combinations of satelite radiance gradients: A theoretical study". United States Naval Postgraduate School, 42 pp.

Kidwell, K., 1979: "NOAA Polar Orbiter Data (Tiros-N) Users Guide". The Satellite Data Services Division.

Lee, D. H., 1979: Level assignment in the assimilation of cloud motion vectors. Mon. Wea. Rev. 107, 1055-1074.

Lorenz, E. N., 1977: An experiment in nonlinear statistical weather forecasting. Mon. Wea. Rev. 105, 590-602.

Phillips, N. A., et al., 1979: An evaluation of early operational temperature sounding from Tiros-N. Bull. Am. Meteorol. Soc. 60, 1188-1197.

Phillips, N. A., 1980: Two examples of satellite temperature retrievals in the North Pacific. Bull. Am. Meteor. Soc. 61, 712-717.

Sampson, R. J., 1978: "Surface II Graphics System". The Kansas Geological Survey, 240 pp.

REFERENCES (Continued)

Smith W. L. and H. M. Woolf, 1976: The use of eigenvectors of statistical covariance matrices for interpreting satellite sounding radiometer observations. J. Atm. Sci. 33, 1127-1140.

Smith, W. L., et al, 1979: The Tiros-N operational vertical sounder. Bull. Amer. Meteor. Soc. 60, 1177-1187.

Zak, J. A., 1967: Estimation of wind in the stratosphere from satellite radiation at 15 microns. M.S. Thesis. Pennsylvania State University.

Zak, J. A., and H. A. Panofsky, 1968: Estimation of stratospheric flow from satellite 15-micron radiation. J. Appl. Meteor. 7, 136-140.

APPENDIX A: FURTHER DETAILS ON TIROS-N RADIANCE DATA PROCESSING

The TOVS System

The new generation NOAA polar orbiter satellite system contains an instrument package which includes an Advanced Very High Resolution Radiometer and the TOVS. The TOVS system includes three sensors, namely the High Resolution Infrared Radiation Sounder (HIRS/2), the Microwave Sounding Unit (MSU), and the Stratospheric Sounding Unit (SSU). A fourth sensor, a backscatter ultraviolet system for ozone measurement, is expected to be added later in the satellite series. Each sensor is a multi-channel radiometer which measures the radiation emerging from the top of the atmosphere. Only the HIRS/2 and MSU data were used in the research discussed in this paper.

The HIRS/2 instrument measures the incident atmospheric radiation in 19 regions of the infrared and one region of the visible part of the spectrum. The three HIRS channels used in this research were channels 3, 4 and 5 which correspond to central wavelengths of 14.5, 14.2, and 14.0 μm respectively. These channels in the 15 μm band provide better sensitivity to the temperature of relatively cold regions of the atmosphere than can be achieved with the 4.3 μm HIRS band channels. Channel 5 radiance values are also used to calculate the heights and amount of cloudiness within the HIRS field of view. The instantaneous fields of view (IFOV) of the HIRS/2 channels are stepped across the satellite track by use of a rotating mirror. This cross-track scan, which covers a linear dimension of about 2240 km, combines with the satellite's motion in orbit to provide coverage over a major portion of the Earth during any 24 hour period. Each individual HIRS/2 measurement (scan spot) results from a 17.4 km diameter circular area at the subsatellite point expanding to approximately a 30x60 km ellipse at larger scan angles. Fifty-six scan

spots comprise one scan line, which is achieved by each mirror rotation. A sounding is then extracted for every array of seven scan lines and nine scan spots through a weighting technique. The result is a 5 x 6 array of data for each 40 x 56 array of scan spots. A calibration every 256 seconds (40 mirror rotations) replaces the measurements for 3 scan lines causing a larger than normal spacing between data at the end of the 256 second period. Thus, the along track data points are arranged in a series of 5 points about 250 km apart, with roughly a 35% greater spacing between the groups of five.

The MSU sensor is a passive scanning microwave spectrometer with 4 channels in the 5.5 micrometer region of the spectrum. The two channels used in this research (channels 2 and 3) respond to 53.74 and 54.96 GHz frequencies. The microwave channels probe through clouds and are used to negate the influence of clouds on the 4.3 μm and 15 μm HIRS channels. The MSU has a wider FOV than the HIRS, accounting for only eleven FOV along its 2240 km swath. MSU soundings are extracted in a similar fashion to that used for the HIRS with the MSU measurements interpolated to the HIRS scan positions hence constituting a similar grid as the HIRS.

Data Processing

The transformation of radiances measured in the 24 spectral intervals of the TOVS system (20 HIRS, 4 MSU) into vertical profiles of atmospheric temperature is accomplished through the operation of 4 principal software modules on an IBM 360/195 computer system. A brief discussion of 2 of these modules, namely the Preprocessor and the Tiros Atmospheric Radiance Module (TARM) follows.

The Preprocessor organizes the output of the TOVS data into a form which is convenient for scientific processing. Input to this module consists of

time coincident sets of HIRS and MSU measurements with earth location and calibration equations appended. These data are representative of the radiation emitted from the top of the atmosphere.

The major function of TARM is to transform the individual FOV data provided by the Preprocessor into sets of atmospheric radiances for determination of atmospheric parameters by the Tiros Retrieval Module (TRET).

The Preprocessor output for both the HIRS and MSU data is organized to allow formation of boxes whose dimensions are 9 scan spots across the satellite track by 7 scan spots along the track. Subsequent operations performed within TARM are in terms of these FOV ensembles. These operations aim to produce a single set of radiances in the 24 spectral intervals of HIRS and MSU, from which an atmospheric sounding can be obtained in TRET.

The physical problem addressed in TARM is the extraction of the true thermal emission of the atmosphere within the volume being sampled from the collection of radiance measurements. Since there are likely to be clouds over such a region and since up to 50% of the HIRS spectral measurements in channel 3, for example, are subject to contamination by clouds, this endeavor is known as the clear column radiance problem. This cloud contamination occurs in HIRS channels which have weighting function peaks in the mid-troposphere where clouds greatly affect radiance measurements.

There are two basic approaches to the clear column radiance problem. First, an attempt is made to find holes in the clouds where uncontaminated observations can be obtained. Second, statistical techniques can be applied in order to infer clear column radiances from the contaminated ensemble. Both methods are utilized in TARM.

Initially, the observations for each FOV in a box are given objective tests to determine the probable presence of clouds. These tests, which are

related only indirectly to cloud amount, involve comparison of the measured reflectance with the expected surface albedo, longwave and shortwave window channel comparisons, longwave window brightness temperature and expected surface temperature comparisons and an infrared-based regression estimate of the microwave brightness temperature and the observed microwave brightness temperature. The expected surface temperature is obtained from analyses of ships and satellite sea surface temperatures as well as shelter land temperatures. Since the vertical weighting functions of several tropospheric-sensing HIRS channels bracket those of the MSU channels, the regression test gives physical reasoning to expect accuracy in predicting the HIRS radiance from MSU measurements in the absence of clouds. However, in the presence of clouds, the HIRS predicted MSU radiance will be too low.

A box is considered to be clear if as few as 4 of the 63 FOVs are found to be clear. The clear value for each of the parameters associated with the box is a weighted average over the clear FOVs. In the event that fewer than four clear FOVs are found in the initial search, a second approach, the so-called adjacent pair or N* technique is employed.

The specification of "cloud-free" infrared radiances from cloud-contaminated observations is performed by using the "paired field of view" method. This technique assumes that the variation of radiance observed in two neighboring fields of view is caused explicitly by a variation of cloud amount. In this situation the cloud free radiance R_j is given by

$$R_j = \frac{R_{1,j} - N^* R_{2,j}}{1 - N^*} \qquad (1)$$

where the subscript j refers to the spectral channel and the numerical subscripts refer to the two geographical fields of view. The parameter N* is the ratio of cloud amounts, N_1/N_2, in the two fields of view. For the Tiros N, it is desirable to make use of the radiance observed in microwave channels, which penetrate clouds, in the specification of clear-column infrared radiances. Through the use of radiance eigenvectors, a simultaneous equation for N* can be obtained and the clear column radiances of all channels can also be obtained as functions of the radiances observed in all channels, infrared and microwave.

The use of these eigenvectors produces solutions that are optimal for the number of parameters used in a statistical sense.

The minimum number of acceptable pairs for N* success is four. The output is a weighted average, with the weight for each pair being proportional to the reciprocal of the error in the regression estimate of the MSU brightness temperature based upon the HIRS clear column radiance determination.

In the event that both the clear search and the adjacent pair method fail, the output for the 63 FOV box is taken as a spatial average of the MSU channels and the stratospheric based HIRS channels (i.e., those presumed not subject to cloud contamination).

The final result is a grid encompassing the North American continent with radiances covering the network (grid) at a horizontal resolution of about 250 km.

APPENDIX B: SINGLE CHANNEL MAPPINGS FROM THE DEVELOPMENTAL SAMPLE

This is a selection of single channel radiance maps drawn for the 21-day developmental sample. The purpose of the inclusion of this set of maps is two-fold.

1) Maps of radiance contours with raw radiance values plotted are included to give the reader a feeling for the density and distribution of observations in the five channels used. The maps presented here are from relatively data rich days. Even on these data rich days, gaps in the data are evident especially for HIRS 5 whose peak energy contribution comes from the middle troposphere. It's sensitivity to clouds is thus apparent. While the number of observations in HIRS channels 3 and 4 is somewhat better, the gradients are much weaker rendering their information less useful.

2) Maps of radiance contours with shear arrows are included to supplement the maps in the body of the text. These show additional examples of the correspondence between radiance gradients in various channels with wind shear in the middle troposphere. It is interesting to note that in the maps presented here, cross contour departures appear to be most prevalent on the eastern part of the maps. This may be partially accounted for by the fact that time correspondence between radiance observation and wind shear observations is poorest in these locations. Thus, especially with rapidly translating systems, systematic departures here may be expected.

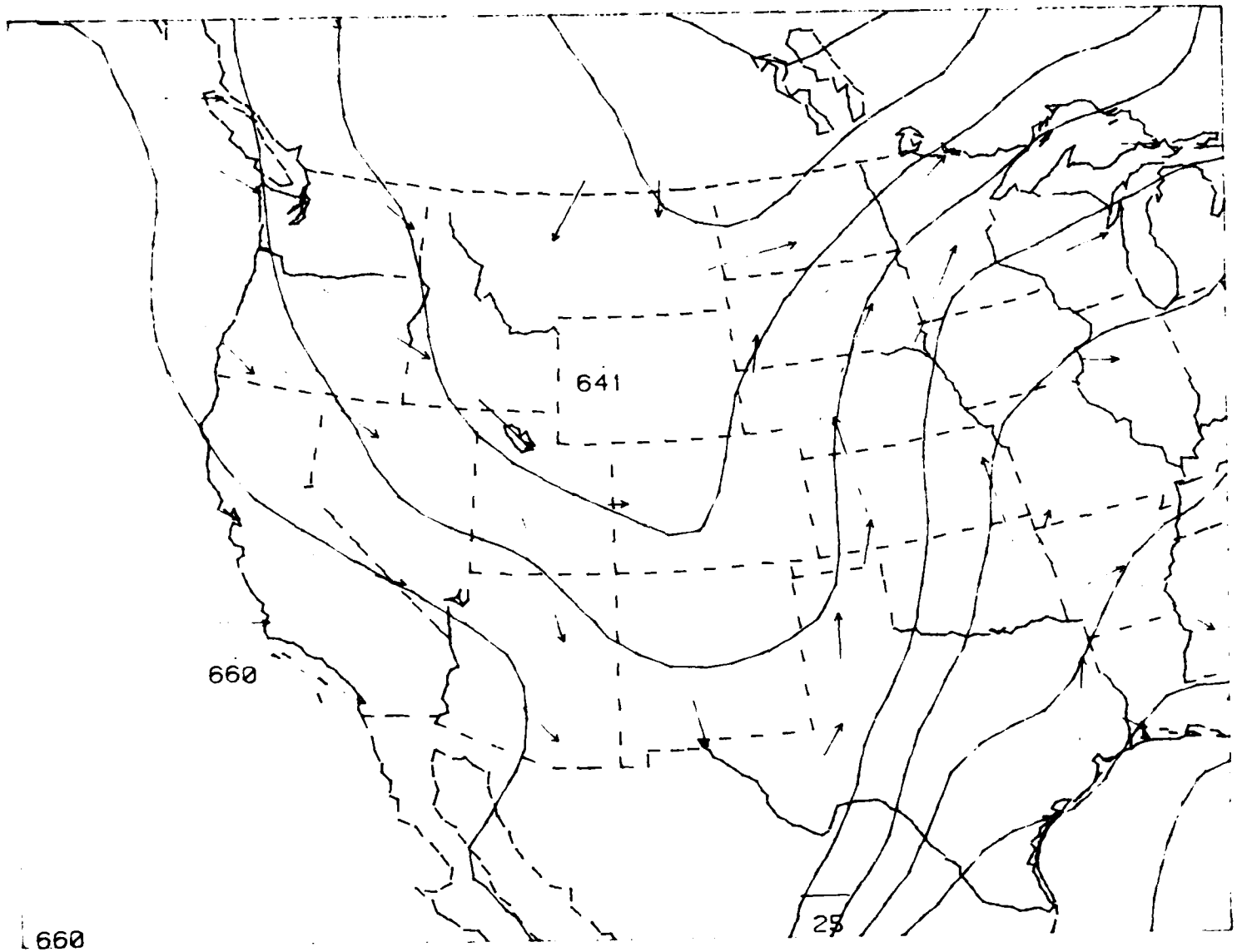

Figure 7. MSU channel 2 radiance contours (descending node) with 400-850 mb wind shear arrows at 1200 GMT 3 March 1979. Radiances in milliwatts per m^2 per steradian per cm^{-1} ($x10^{-5}$). Contour interval = 100.

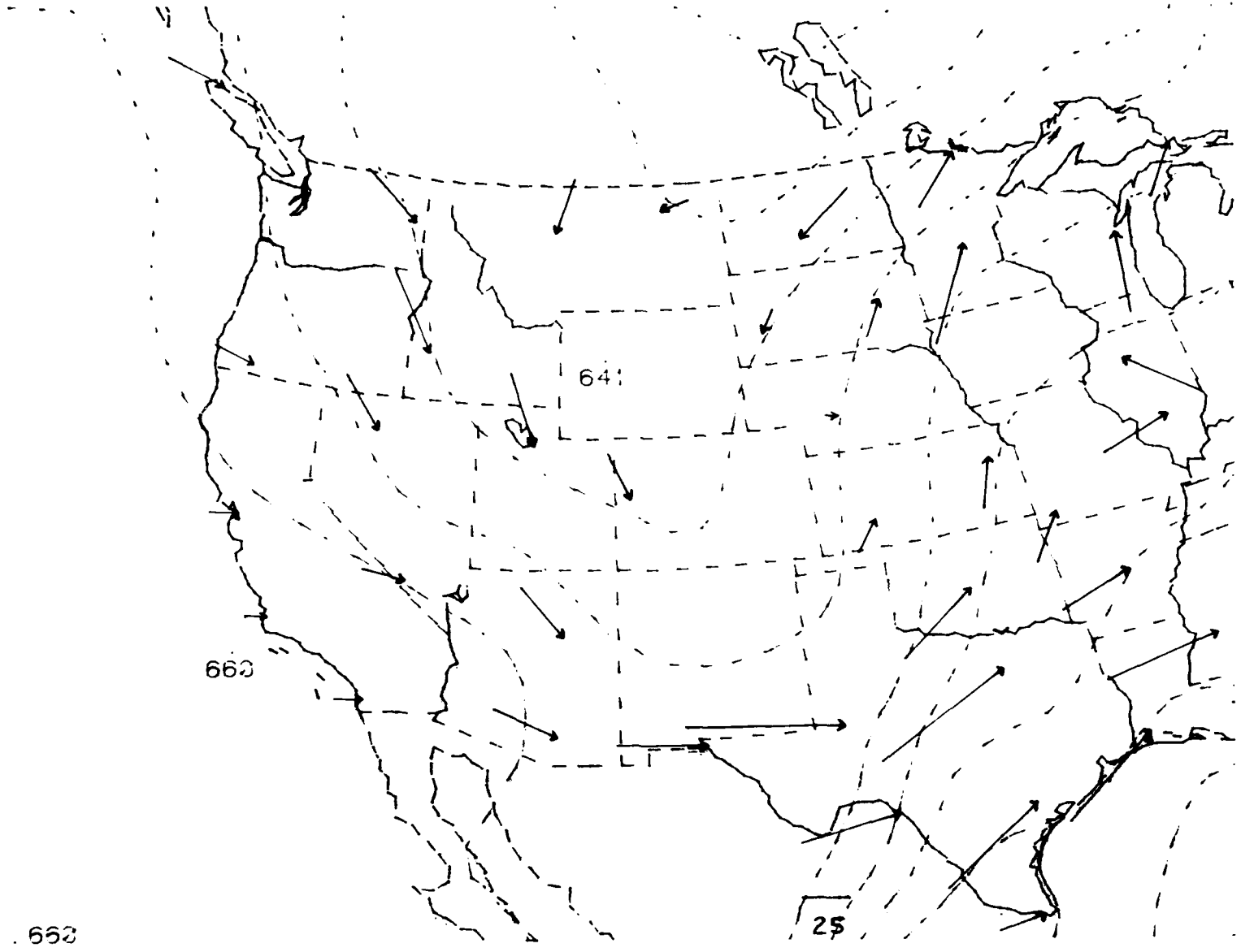

Figure 8. MSU channel 2 radiance contours (descending node) with 400-850 mb wind shear arrows at 1200 GMT 4 March 1979. Radiances in milliwatts per m^2 per steradian per cm^{-1} ($x10^{-5}$). Contour interval = 100.

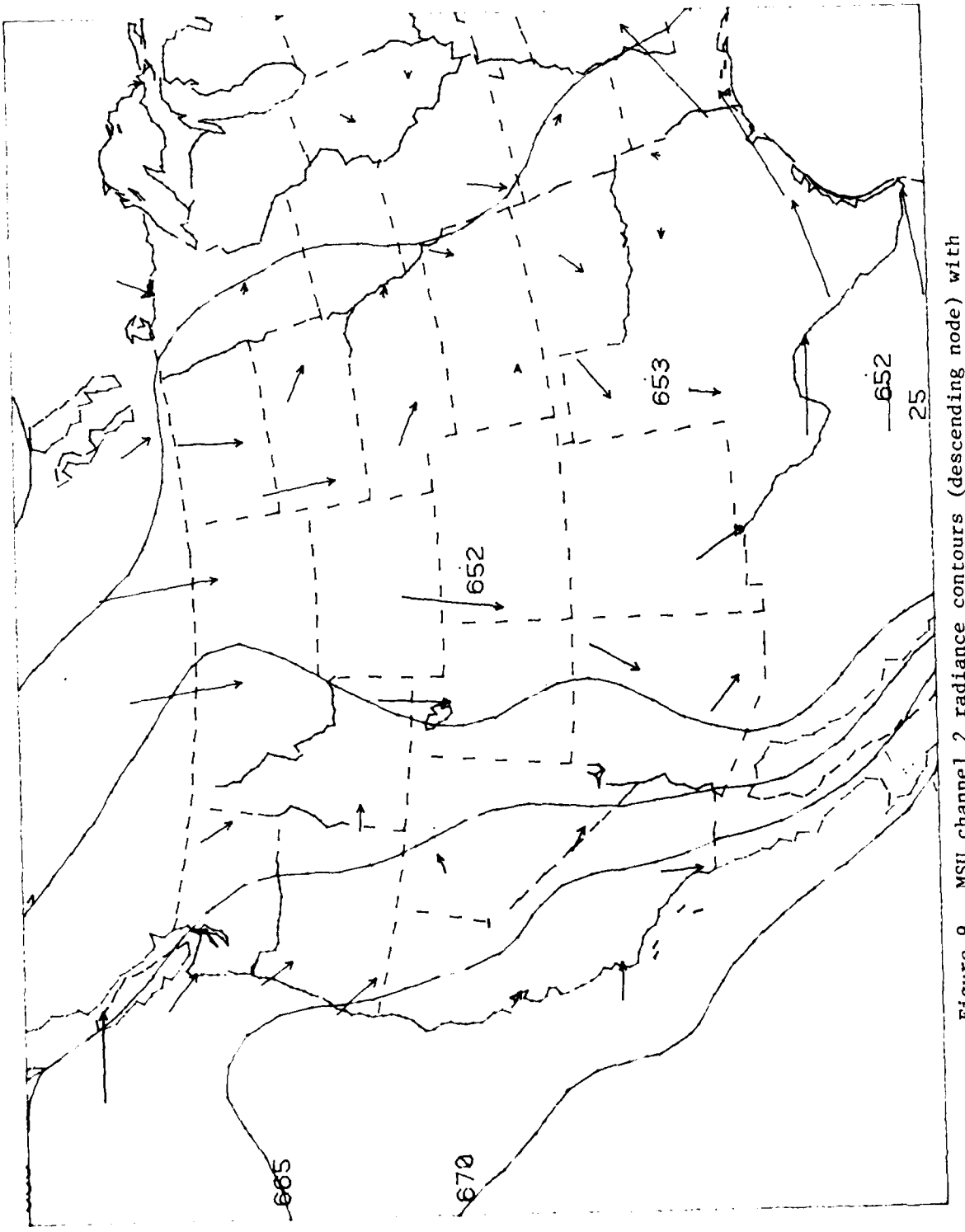

Figure 9. MSU channel 2 radiance contours (descending node) with 400-850 mb wind shear arrows at 1200 GMT 6 March 1979. Radiances in milliwatts per m^2 per steradian per cm^{-1} ($x10^{-5}$). Contour interval = 100.

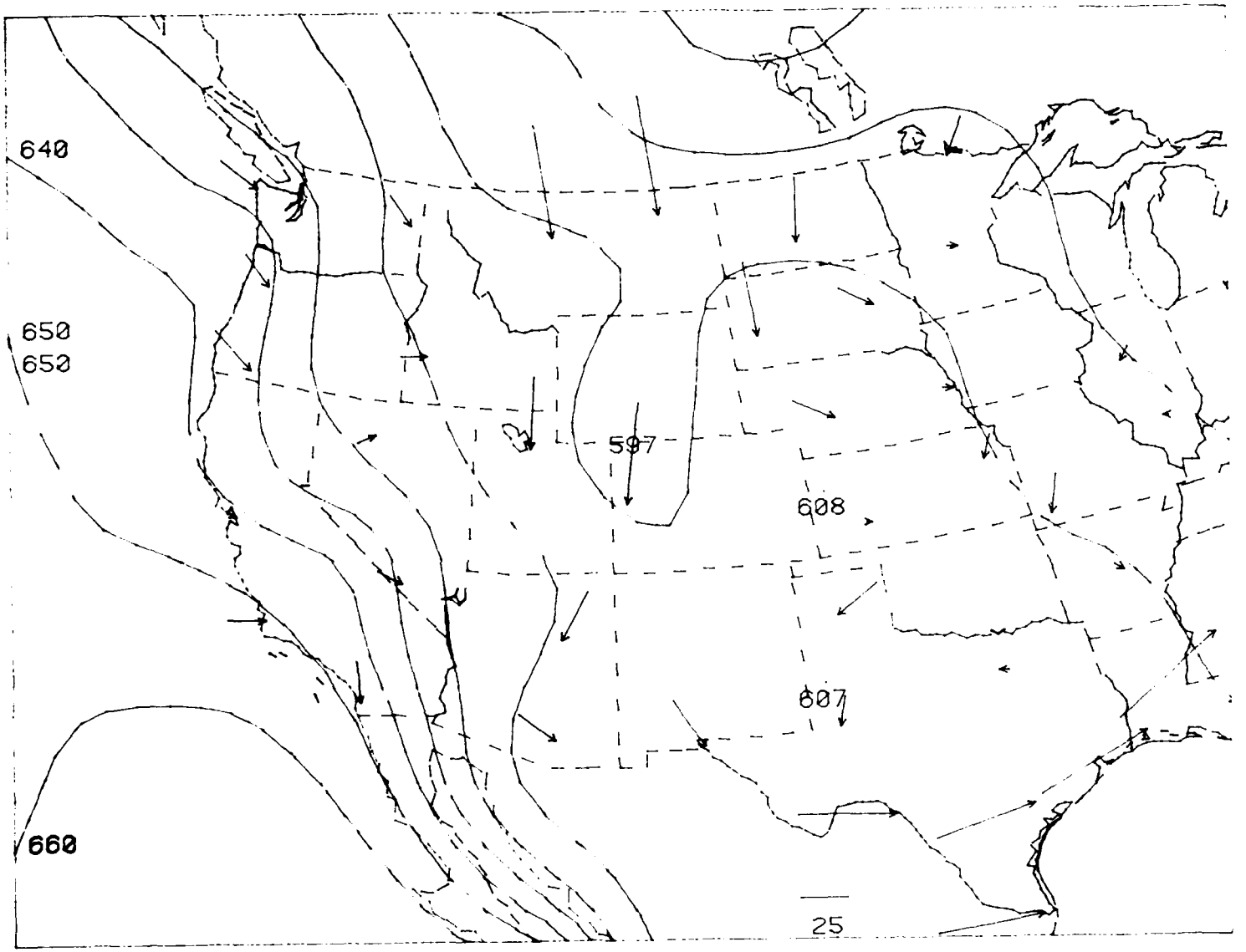

Figure 10. HIRS channel 5 radiance contours (descending node) with 400-850 mb wind shear arrows at 1200 GMT 6 March 1979. Radiances in milliwatts per m^2 per steradian per cm^{-1} ($x10^{-1}$). Contour interval = 50.

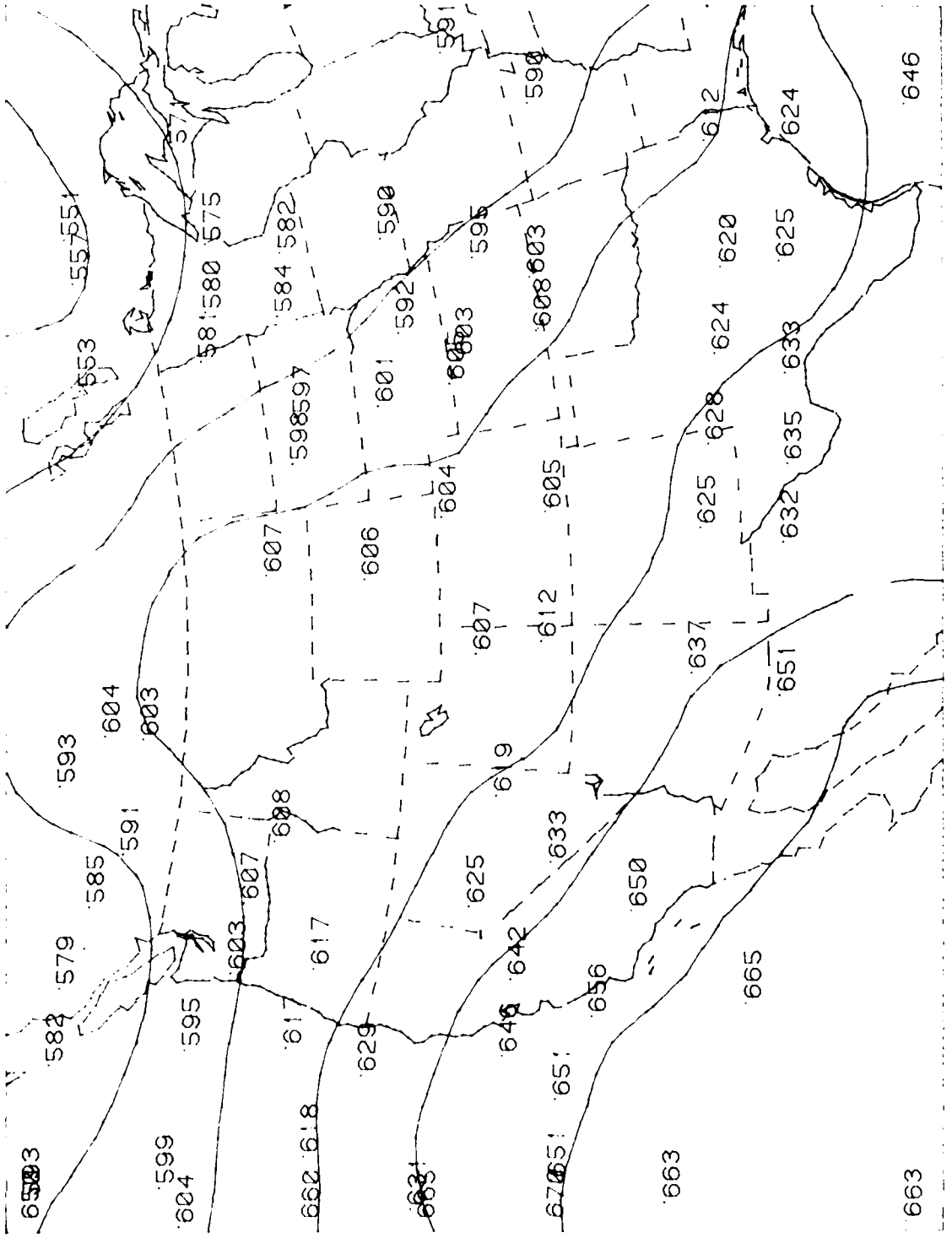

Figure 11. MSU channel 2 radiance contours (descending node, 7 March 1979) with radiance values from TARM plotted. Radiances in milliwatts per m^2 per steradian per cm^{-1} ($x10^{-5}$). Contour interval = 100.

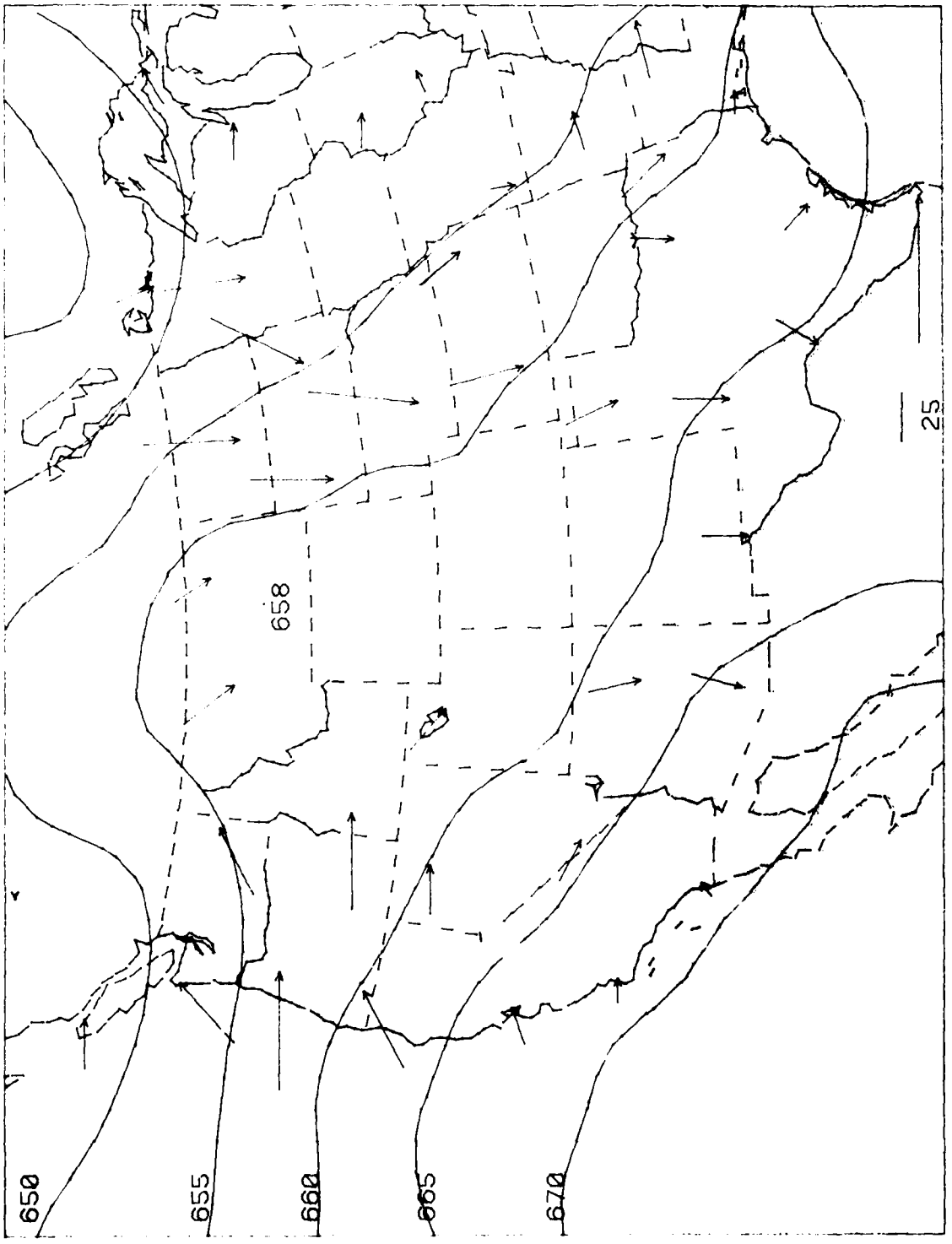

Figure 12. MSU channel 2 radiance contours (descending node) with 400-850 mb wind shear arrows at 1200 GMT 7 March 1979. Radiances in milliwatts per m^2 per steradian per cm^{-1} ($x10^{-5}$). Contour interval = 100.

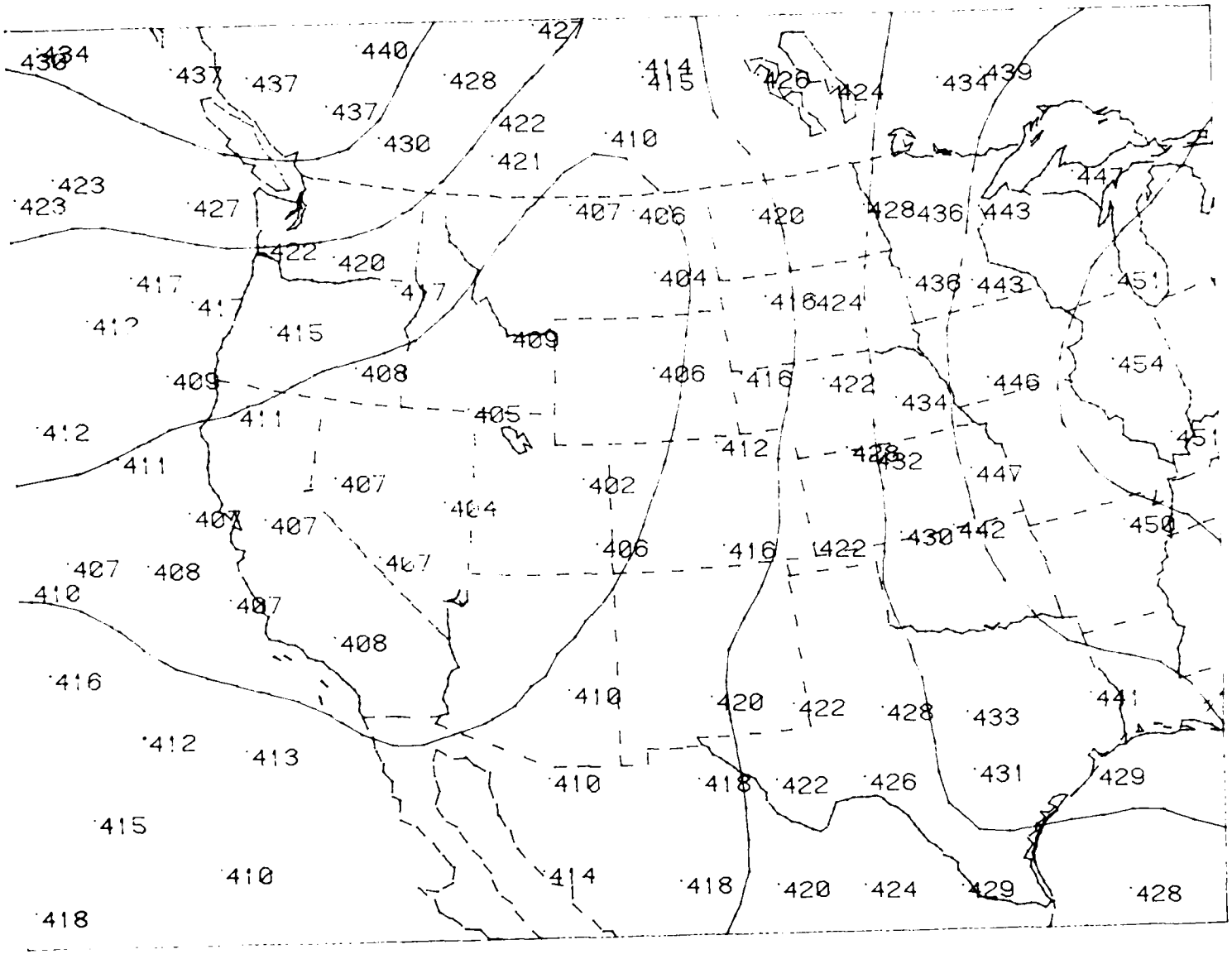

Figure 13. HIRS channel 3 radiance contours (descending node, 7 March 1979) with radiance values from TARM plotted. Radiances in milliwatts per m ^{2} per steradian per cm^{-1} (x10^{-1}). Contour interval = 50.

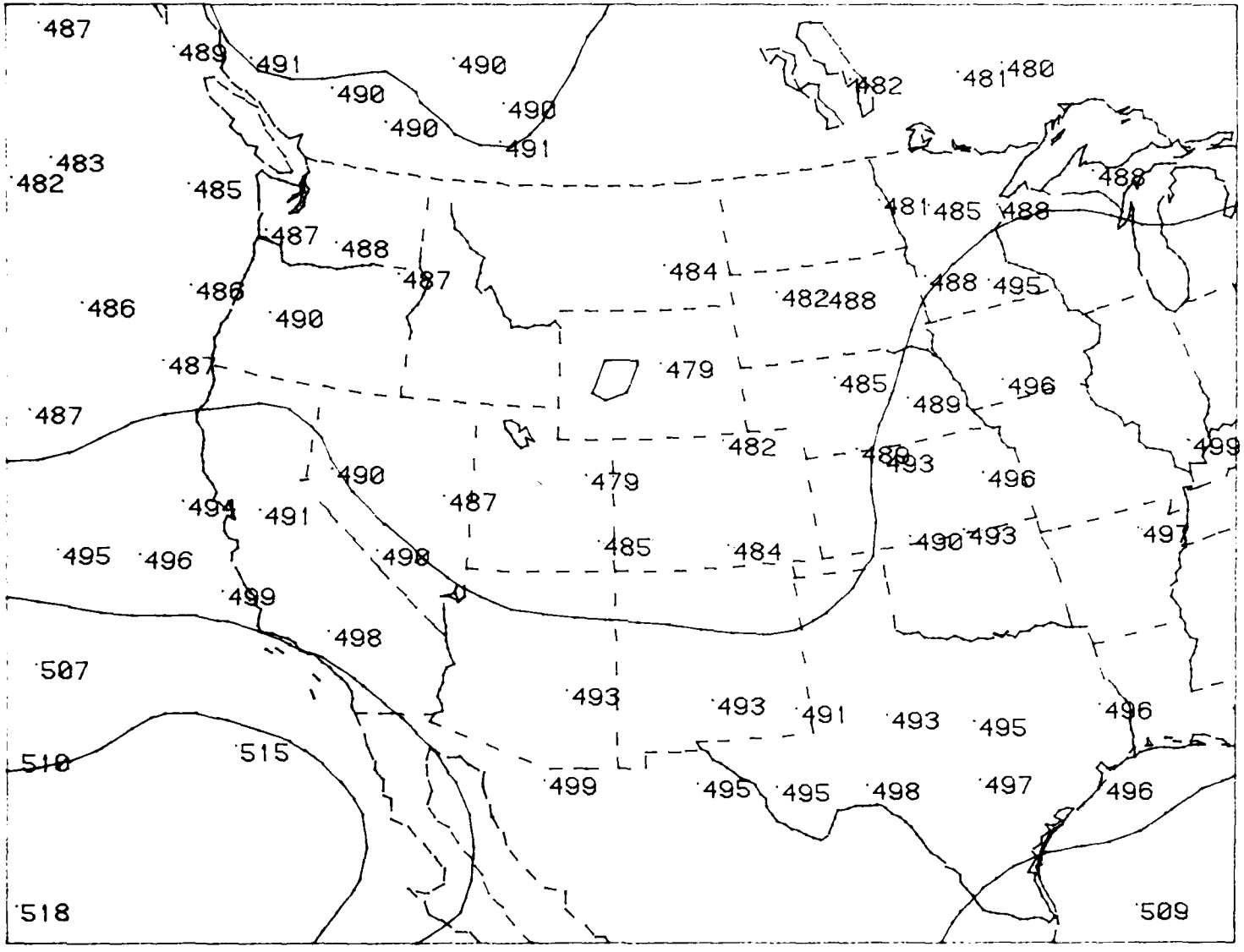

Figure 14. HIRS channel 4 radiance contours (descending node, 7 March 1979) with radiance values from TARM plotted. Radiances in milliwatts per m^2 per steradian per cm^{-1} ($x10^{-1}$). Contour interval = 50.

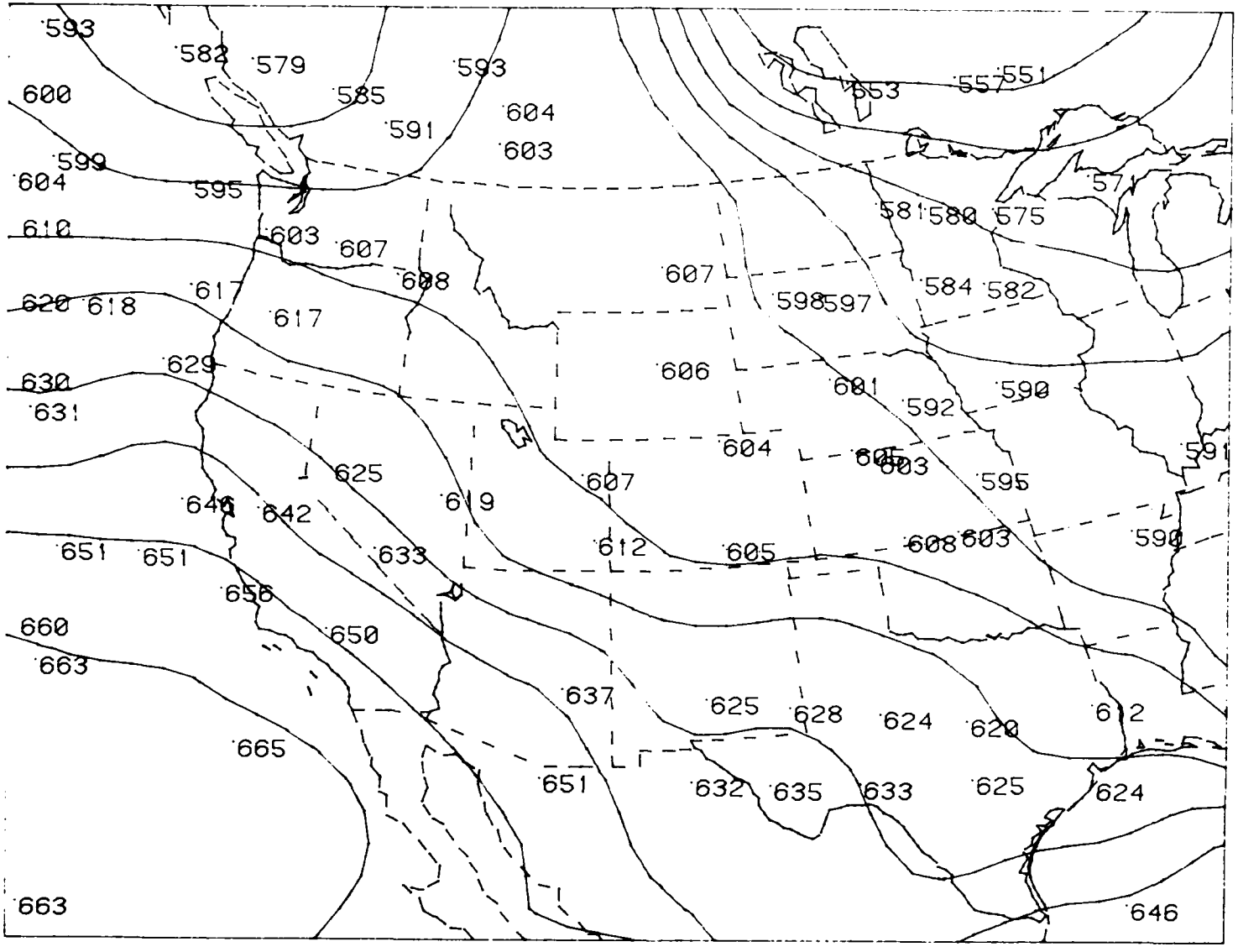

Figure 15. HIRS channel 5 radiance contours (descending node, 7 March 1979) with radiance values from TARM plotted. Radiances in milliwatts per m^2 per steradian per cm^{-1} ($x10^{-1}$). Contour interval = 50.

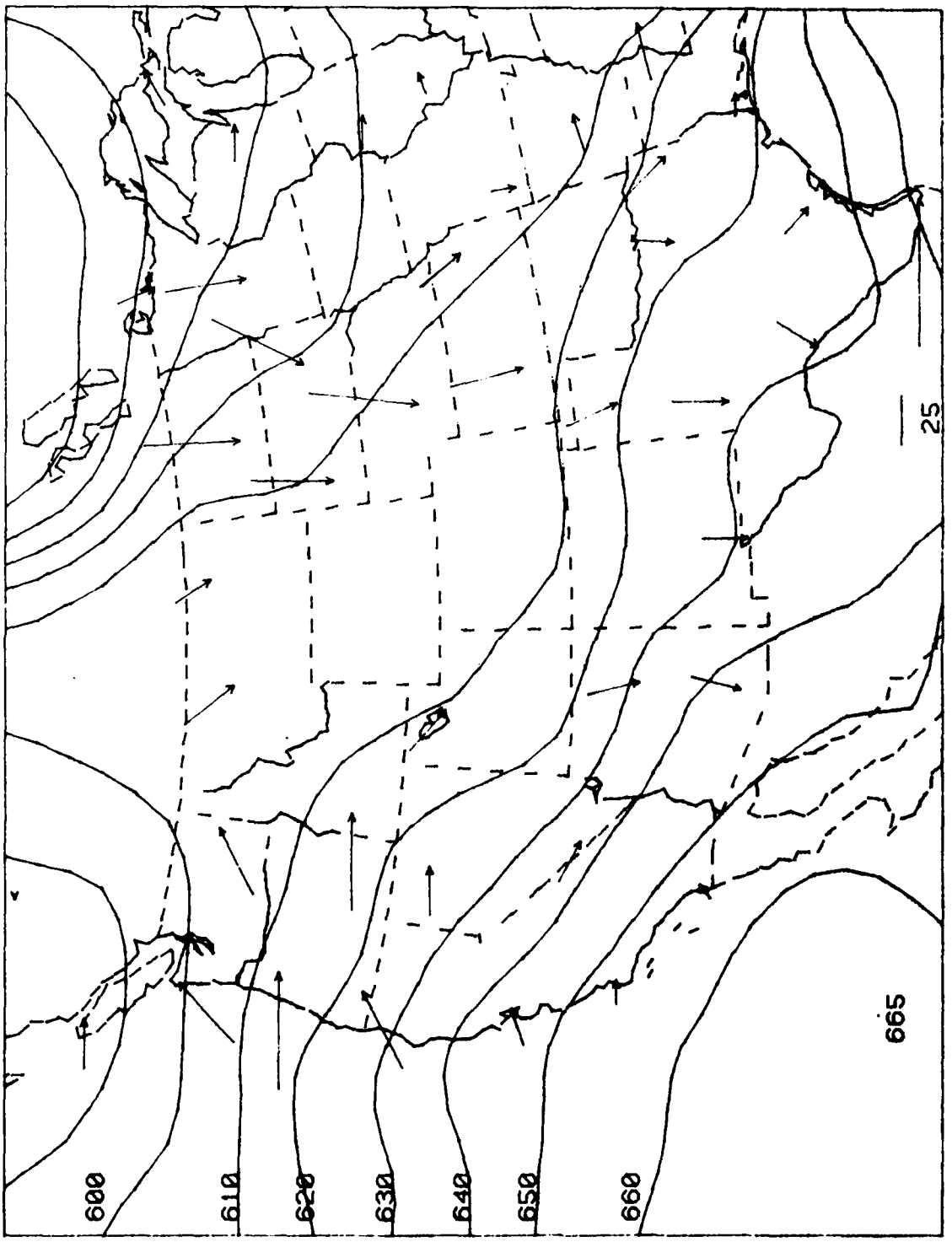

Figure 16. HIRS channel 5 radiance contours (descending node) with 400-850 mb wind shear arrows at 1200 GMT 7 March 1979. Radiances in milliwatts per m^2 per steradian per cm^{-1} ($x10^{-1}$). Contour interval = 50.

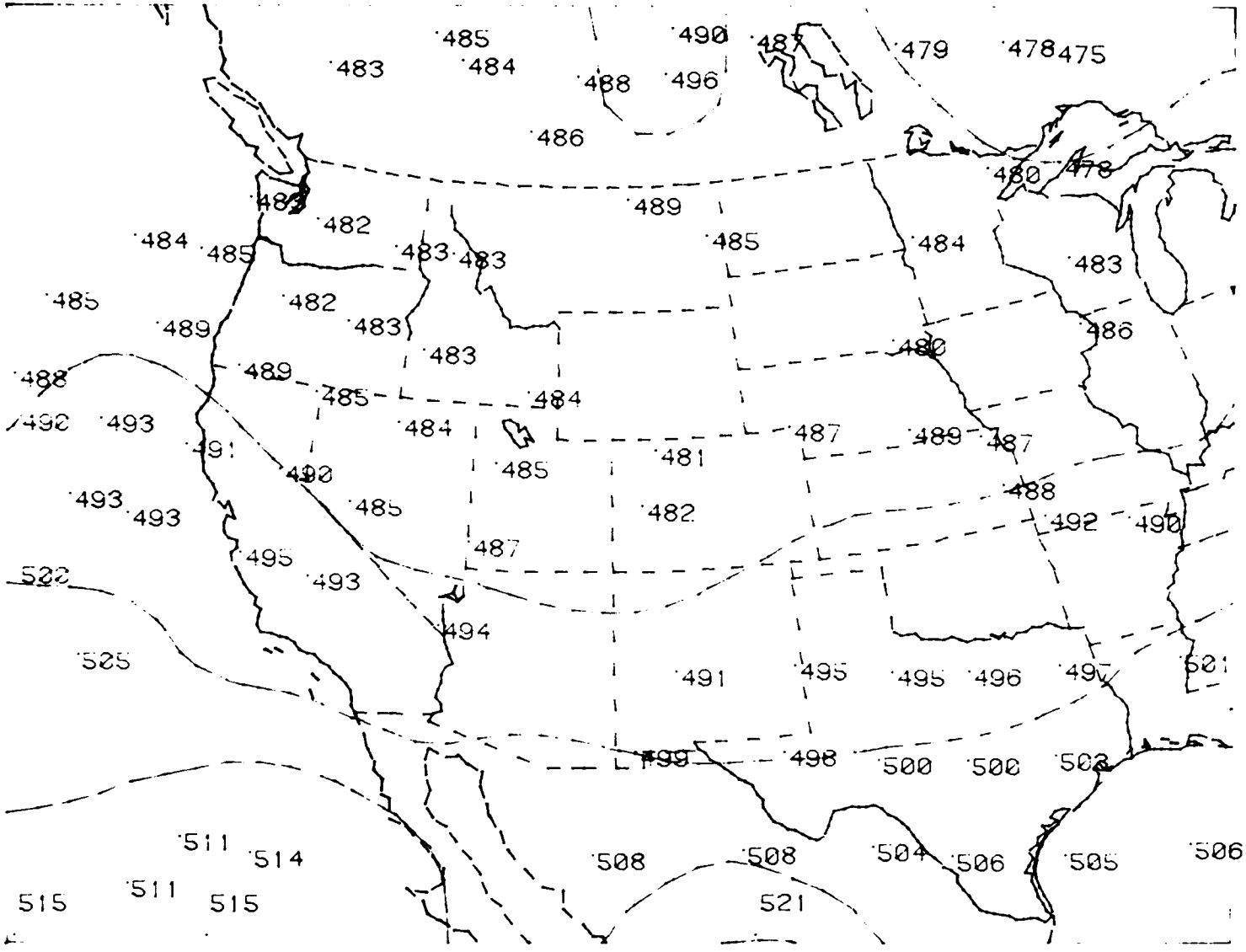

Figure 17. HIRS channel 3 radiance contours (descending node, 8 March 1979) with radiance values from TARM plotted. Radiances in milliwatts per m ^{2} per steradian per cm^{-1} (x10^{-1}). Contour interval = 50.

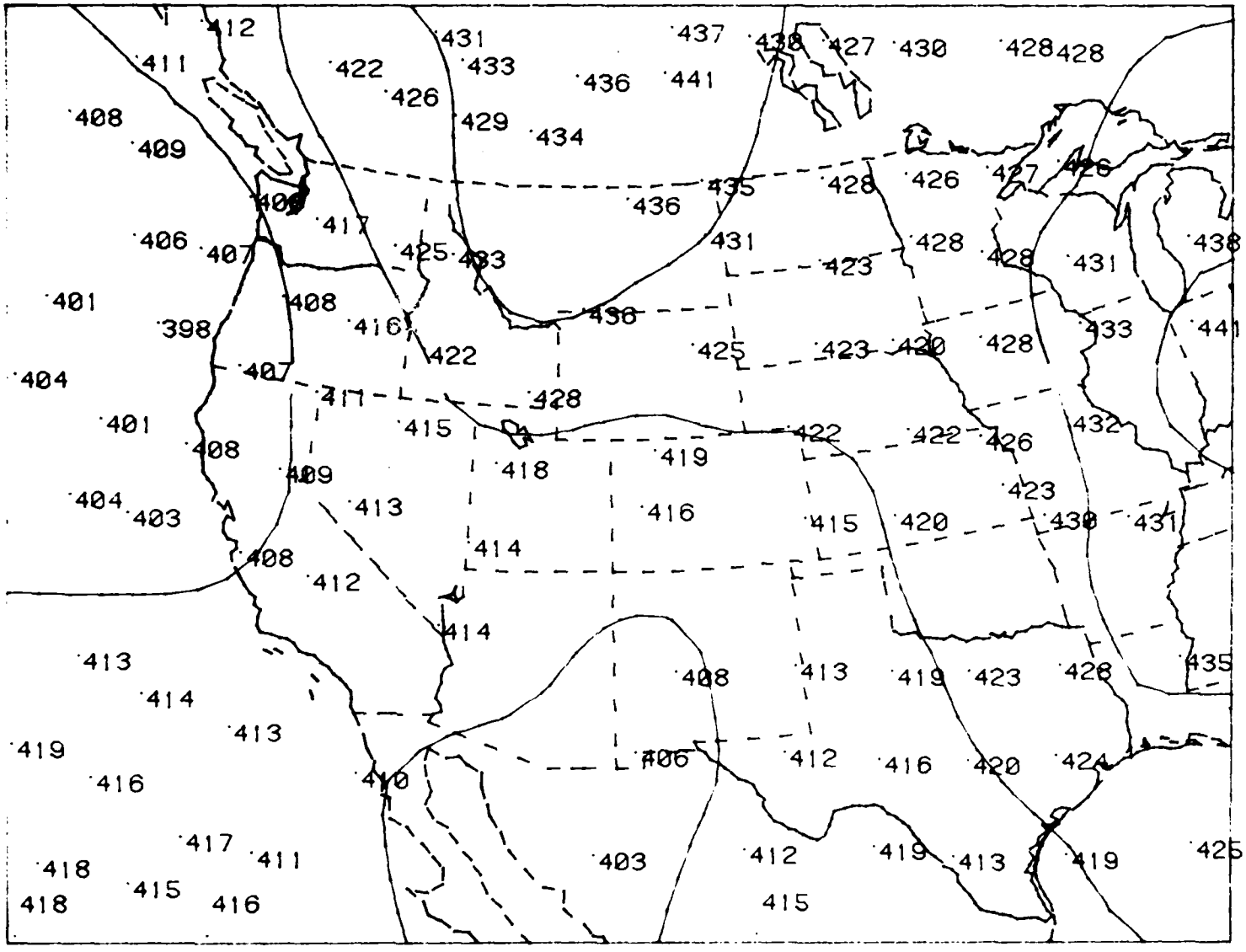

Figure 18. HIRS channel 4 radiance contours (descending node, 8 March 1979) with radiance values from TARM plotted. Radiances in milliwatts per m^2 per steradian per cm^{-1} ($x10^{-1}$). Contour interval = 50.

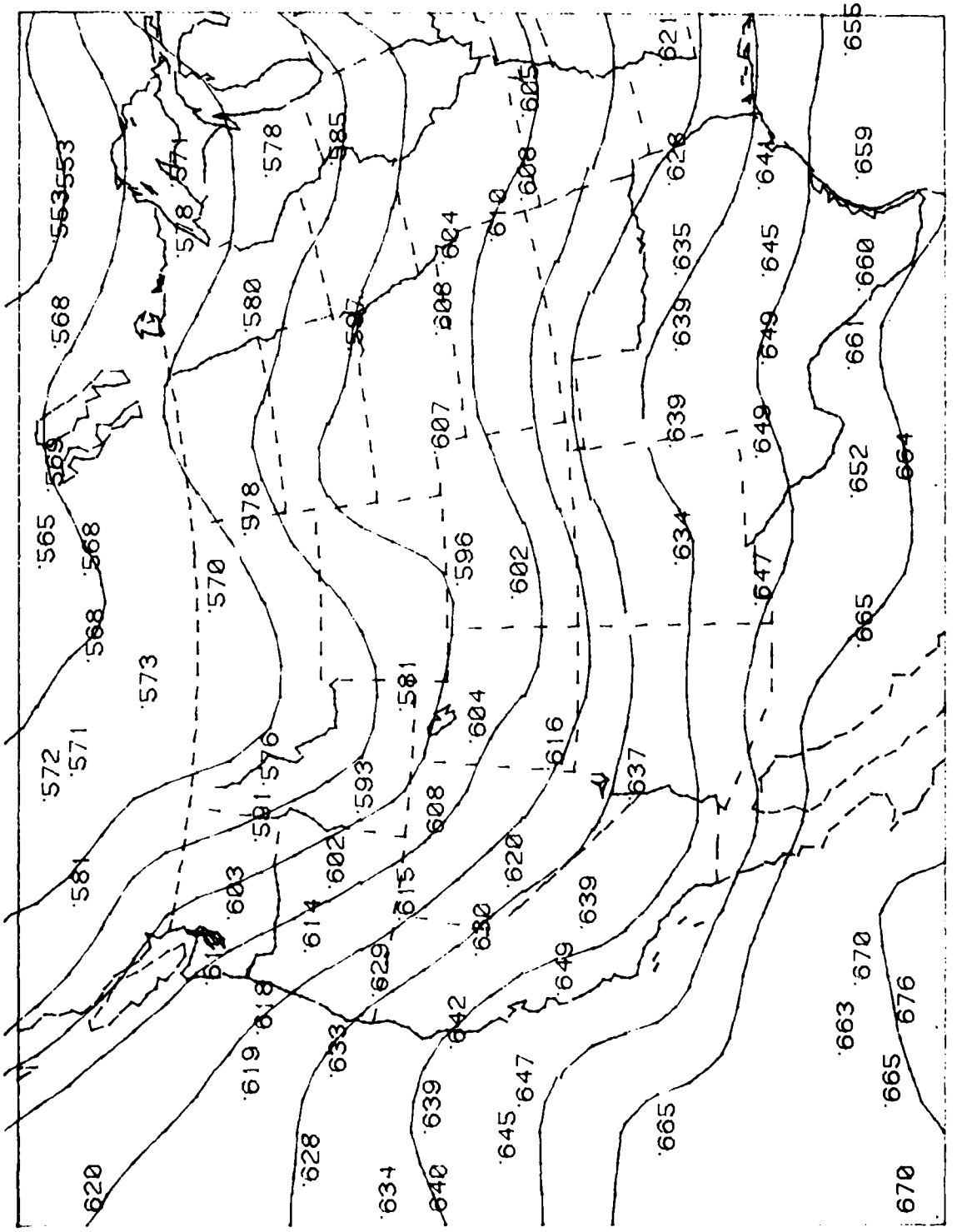

Figure 19. HIRS channel 5 radiance contours (descending node, 8 March 1979) with radiance values from TARM plotted. Radiances in milliwatts per m^2 per steradian per cm^{-1} ($x10^{-1}$). Contour interval = 50.

APPENDIX C: SUMMARY OF REGRESSION COEFFICIENTS

This appendix is a complete summary of all of the regression coefficients for all layers and combinations of channels for which equations were developed. The equations presented here include coefficients for predictors which entered the regression equations at the $\alpha = 0.1$ significance level or higher. It must be remembered that these equations were developed from a limited data base consisting of approximately 275 observations. Thus, the coefficients are likely to be quite unstable. The predictands are observed wind shears (in knots) between the mandatory levels indicated or winds (in knots) at the single level indicated. Predictors are microwave and infrared radiances in milliwatts per m^2 per steradian per cm^{-1} per 100 km) for various channels on the TOVS instruments.

USH 2540 = 3.2 + 43.7 MSU2 + 2625 HIRS4 + 1336 HIRS5
VSH 2540 = 1.9 + 42.9 MSU2 + 1236 HIRS4
USH 2550 = 3.6 + 75.1 MSU2 + 2218 HIRS4 + 1986 HIRS5
VSH 2550 = 0.7 + 81.4 MSU2 - 54.6 MSU3 + 1647 HIRS4
USH 2570 = 7.4 + 123 MSU2 + 2328 HIRS4 + 2105 HIRS5 - 2478 HIRS3
VSH 2570 = 0.5 + 150 MSU2 - 115 MSU3 + 1654 HIRS4
USH 2585 = 10.6 + 154 MSU2 + 3788 HIRS5 - 2462 HIRS3
VSH 2585 = 0.4 + 201 MSU2 - 164 MSU3 + 1662 HIRS4
USH 3050 = 1.4 + 67.8 MSU2 + 1890 HIRS5
VSH 3050 = 1.3 + 80.6 MSU2 - 55 MSU3
USH 3070 = 3.6 + 129 MSU2 - 120 MSU3 + 2233 HIRS5
VSH 3070 = 1.2 + 150 MSU2 - 118 MSU3
USH 3085 = 7.2 + 160 MSU2 - 110 MSU3 + 2987 HIRS5 - 2119 HIRS3
VSH 3085 = -0.9 + 184 MSU2 - 162 MSU3
USH 7085 = 3.2 + 366 MSU2 + 551 HIRS5 - 999 HIRS3
VSH 7085 = -1.8 + 35 MSU2 - 423 MSU3
USH 2050 = 9.2 + 56 MSU2 + 114 MSU3 + 2203 HIRS4 + 934 MSU5
VSH 2050 = 0 + 45 MSU2 + 35.5 MSU3 - 501 HIRS5

USH 2070 = 12.8 + 101 MSU2 + 3383 HIRS4 + 1129 HIRS5 - 2208 HIRS3

VSH 2070 = -0.8 + 100.5 MSU2

USH 2085 = 14.8 + 148 MSU2 - 85.4 MSU3 + 2768 HIRS5 - 2297 HIRS3

VSH 2085 = 2.4 + 143 MSU2 - 56.8 MSU3

USH 4085 = 7.2 - 111 MSU3 + 114 MSU2 + 1528 HIRS5 - 2718 HIRS3

VSH 4085 = -0.5 + 216 MSU2 - 184 MSU3

USH 4070 = 4.2 + 76.9 MSU2 - 93.1 MSU3 + 811 HIRS5 - 1954 HIRS3

VSH 4070 = 0.6 + 192 MSU2 - 174 MSU3

USH 5070 = 3.5 + 53.6 MSU2 - 56.3 MSU3 - 1474 HIRS3

VSH 5070 = -0.8 + 57 MSU2 - 56 MSU3 + 409 HIRS5

Equations for single levels:

U200 = 22 + 131 MSU2 + 2009 HIRS5 - 2184 HIRS3

V200 = 0.6 + 167 MSU2 - 134.4 MSU3

U300 = 11.9 + 160 MSU2 - 227 MSU3 + 2679 HIRS5

V300 = 2.5 + 203 MSU2 - 218 MSU3

U500 = 10.5 + 92.2 MSU2 - 175 MSU3 + 898 HIRS5

V500 = 1.3 + 129 MSU2 - 170 MSU3

DISTRIBUTION

SPECIAL ASST. TO THE ASST.
SECNAV (R&D)
RM. 4E741, THE PENTAGON
WASHINGTON, DC 20350

CHIEF OF NAVAL OPERATIONS
OP-952
U.S. NAVAL OBSERVATORY
WASHINGTON, DC 20390

CHIEF OF NAVAL OPERATIONS
NAVY DEPT. OP-986
WASHINGTON, DC 20350

NAVAL DEPUTY TO THE ADMIN.
NOAA, RM. 200, PAGE BLDG. #1
3300 WHITEHAVEN ST. NW
WASHINGTON, DC 20235

OFFICER IN CHARGE
NAVOCEANCOMDET
AFGWC
OFFUTT AFB, NE 68113

COMMANDING OFFICER
NORDA, CODE 101
NSTL STATION
BAY ST. LOUIS, MS 39529

COMMANDER
NAVOCEANCOM
NSTL STATION
BAY ST. LOUIS, MS 39529

COMMANDING OFFICER
FLENUMOCEANCEN
MONTEREY, CA 93940

COMMANDER
NAVAIRSYSCOM
ATTN: LIBRARY, AIR-00D4
WASHINGTON, DC 20361

COMMANDER
NAVAIRSYSCOM (AIR-370)
WASHINGTON, DC 20361

NAVAL POSTGRADUATE SCHOOL
METEOROLOGY DEPT., CODE 63
MONTEREY, CA 93940

NAVAL POSTGRADUATE SCHOOL
ATTN: LIBRARY
MONTEREY, CA 93940

USAFETAC/TS
SCOTT AFB, IL 62225

AFGL/LY
HANSCOM AFB, MA 01731

AFOSR/NC
BOLLING AFB
WASHINGTON, DC 20312

DIRECTOR
DEFENSE TECHNICAL INFORMATION
CENTER (DTIC)
CAMERON STATION
ALEXANDRIA, VA 22314

NATIONAL METEOROLOGICAL CENTER
DEVELOPMENT DIVISION
NWS/NOAA
WORLD WEATHER BLDG. W32, RM 204
WASHINGTON, DC 20233

DIRECTOR
NATIONAL EARTH SAT. SERV./SEL
FB-4, S321B
SUITLAND, MD 20233

NATIONAL WEATHER SERVICE
WORLD WEATHER BLDG., RM. 307
5200 AUTH ROAD
CAMP SPRINGS, MD 20023

DIRECTOR
NATIONAL SEVERE STORMS LAB
1313 HALLEY CIRCLE
NORMAN, OK 73069

CHIEF
NATIONAL EARTH SATELLITE SERV.
MESOSCALE APPLICATIONS BRANCH
1225 W. DAYTON
MADISON, WI 53562

NATIONAL CENTER FOR ATMOSPHERIC
RESEARCH
LIBRARY ACQUISITIONS
P.O. BOX 1470
BOULDER, CO 80302

COLORADO STATE UNIVERSITY
ATMOSPHERIC SCIENCES DEPT.
ATTN: LIBRARIAN
FT. COLLINS, CO 80521

AUSTRALIAN NUMERICAL METEOROLOGY
RESEARCH CENTER
ATTN: DR. R. L. HUGHES
P.O. BOX 5089A
MELBOURNE, VICTORIA
3001 AUSTRALIA

EUROPEAN SPACE OPERATIONS CENTER
ROBERT BOSCH STR. 5
D-61 DARMSTADT
ATTN: DR. J. MORGAN, METEO. SAT.
DATA MANAGEMENT DEPT.
FEDERAL REPUBLIC OF GERMANY

HEAD, DATA PROCESSING SECTION
GERMAN MILITARY GEOPHYSICAL
OFFICE
MOUT-ROYAL, D-5580
TRAVEN-TRARBACH
FEDERAL REPUBLIC OF GERMANY


ATE
MED